Sina Huber
sinahuber@quickline.ch

Romanshorn Upper Secondary School
Class 4Mez
Matura Paper

Solid Gravity Energy Storage: Model Development and Comparative Analysis With Alternative Technologies

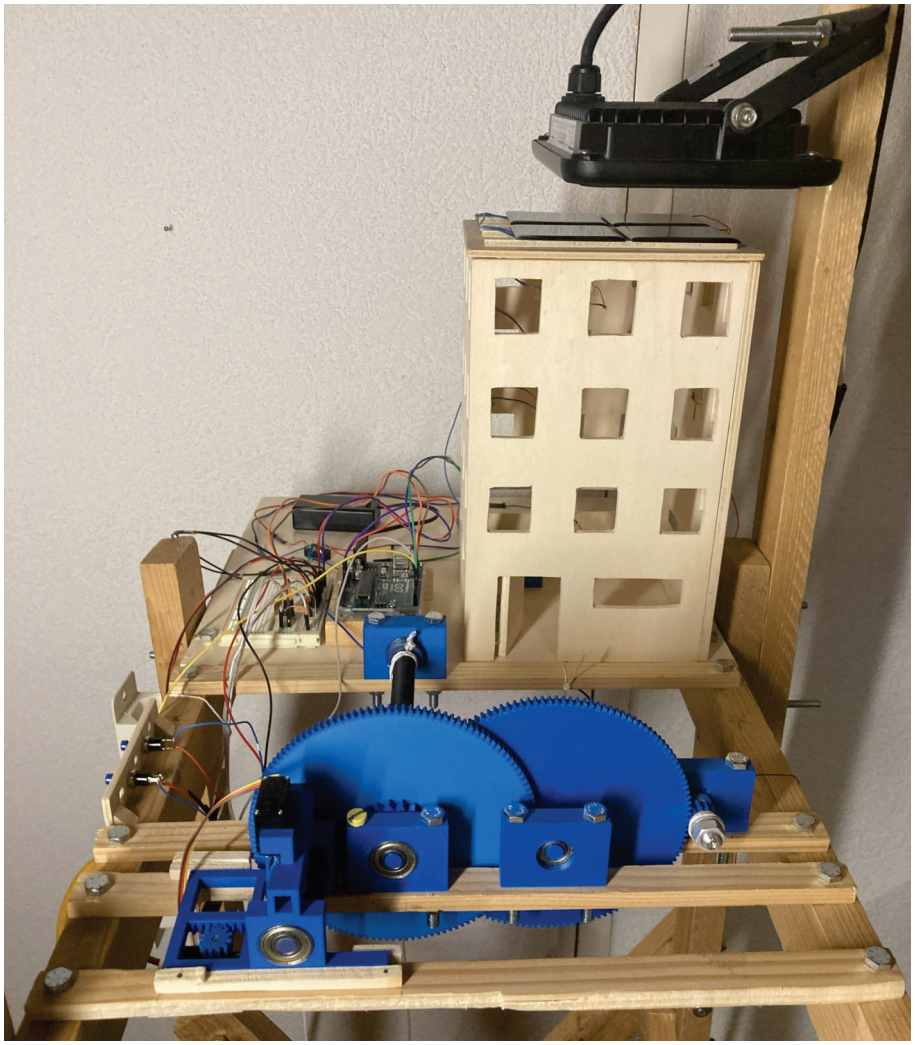

Subject: Physics
Supervisor: Dr. Andreas Schärer
Submitted: 6 January 2025

Abstract

Energy storage technologies are increasingly needed. Innovation is therefore welcomed. One groundbreaking technology is solid gravity energy storage (SGES), which stores energy by increasing the altitude of a mass. It was examined how energy can be stored using weights, and how this method compares with conventional energy storage technologies.

A model of an SGES system was constructed and analysed by measuring the motion of the mass as well as the motor's voltage and its current. The model achieved an efficiency of $6-7\%$ and a maximum energy output of $2.88\,\mathrm{J}$. Furthermore, methods were found to save energy during braking and to achieve constant power more quickly when accelerating at the top. The findings were used to calculate how the model would look in real life. It was found that a mass of $35\,\mathrm{t}$ and an altitude of $100\,\mathrm{m}$ would be needed to store $5\,\mathrm{kWh}$. By researching SGES was compared to other energy storage technologies. This research has shown that, despite their low energy density and lack of maturity, SGES systems have advantages. For instance, they are sustainable and have no self-discharge. This indicates potential for future development of SGES systems.

Contents

1 Introduction

Humans are heavily dependent on electricity in their daily lives and everything that is connected to it, such as the industry and the internet (Zohuri, 2016). Notably, the electricity import and export of Switzerland was mostly balanced over the last twenty years. Often more electricity was exported than imported over a year. However, Switzerland imported around 30 000 GWh electricity per year. In particular, in the winters since 2005, Switzerland imported more electricity than they exported except for one year. (Bundesamt für Statistik, 2023) Furthermore, in the last years renewable energies expanded enormously. Especially wind and solar energy are well represented. However, these two energy sources have a fluctuating output due to changing natural and meteorological conditions. (Wang et al., 2022) These changes in generation and demand can be balanced by energy storage technologies over seconds, hours, or even months. Energy storage can increase self-consumption of solar electricity, and it still provides electricity during a blackout. Additionally, secure and efficient operation of the electricity system is ensured. (European Association for Storage of Energy, 2024b)

There are many different technologies that store electrical energy as chemical, electrochemical, electrical, thermal, or mechanical energy. An example of mechanical energy storage is the solid gravity energy storage technology. (European Association for Storage of Energy, 2024a) The principle of this storage method is to lift masses and let them drop again. Different companies research how this method could be used commercially. Among others, there was a test program built in Ticino by Energy Vault. The goal was to have an energy storage system that fits almost everywhere unlike pumped hydropower energy storage and with lower long-term costs as well as fewer environmental issues than batteries. (Moore, 2021)

This new method to store energy is studied in this paper. On the basis of practical work, the solid gravity energy storage technology is analysed. Additionally, the technology is compared to others based on research. In this paper the following question will be analysed: How can energy be stored using weights, and how does this method compare with conventional energy storage technologies focusing on pumped storage hydropower plants, hydrogen storage, lithium-ion batteries, and vanadium redox flow batteries?

2 Theoretical Framework

This section introduces the types of energy storage relevant to this paper. Additionally, important formulas for the development and the analysis of the model as well as for the comprehension of the topic are listed. Furthermore, important components that were used for the construction of the SGES model are explained.

2.1 Electrical Energy Storage (EES)

The definition of energy storage is the capture and holding of energy in reserve for later use. Electrical energy storage systems support the electric grid. Hence, the electricity demand can be met, although there is not enough electric energy generated. How long an EES system can supply electricity differs. There are some EES systems that supply energy only for a few minutes, such as flywheels. On the contrary, diurnal energy storage systems provide energy for several hours, as do pumped storage hydropower plants. Depending on their type, batteries are either short-duration or diurnal energy storage systems. (Gomstyn & Jonker, 2024)

When electrical energy is stored, it mostly is transformed into a different form of energy. There exist chemical, electrochemical, electrical, mechanical, and thermal EES systems. Each type contains many different energy storage technologies. (European Association for Storage of Energy, 2024a) Some of these different technologies are explained below.

2.1.1 Solid Gravity Energy Storage (SGES)

The basic principle of solid gravity energy storage is lifting a mass up and letting it drop again. There are different companies with different approaches to using gravity to store energy. (Moore, 2021)

In Ticino, Energy Vault built towers with six crane arms (Figure 1) that raise and lower bricks, each of which has a mass of 35 tonnes. These bricks are arranged in concentric rings, and all together can store up to 35 MWh. It was hooked to the grid in 2020. The system possesses a control system, which compensates for gusts of wind. (Moore, 2021)

Figure 1: Energy Vault's project in Ticino, Switzerland (Moore, 2021)

In China, Energy Vault built its two first commercial SGES projects. These have more similarity to a house but still work with cranes (Figure 2). One project was built in Rudong, and it is directly connected to a wind farm and the national grid. It has a storage capacity of 100 MWh. In 2023, they started another project in Zhangye. At the time it is completed, it should store at maximum 68 MWh. (Energy Vault, 2024b,c)

Figure 2: Energy Vault's project in Rudong, China (Energy Vault, 2024b)

Gravitricity is another company that uses a similar principle. Unlike Energy Vault, they use decommissioned mines to build underground energy storage systems. The first large-scale project will be located in central Finland. This project will provide up to 2 MW balancing service to the local grid. (Cuthrell, 2024)

A slightly different approach is SGES aided by water. This technology stores water underground and keeps it under pressure with the help of a piston made of rock. To store electrical energy, water is pumped from a surface water body below the piston. For the generation of electrical energy, the water flows back through a turbine to the surface, due to the pressure created by the piston. (Zahoransky et al., 2019, p. 535) The company Gravity Storage uses this concept (Figure 3). For instance, a piston with a diameter of 150 m and a height of 187.5 m could store 1.3 GWh of energy. (Gravity Storage, 2024)

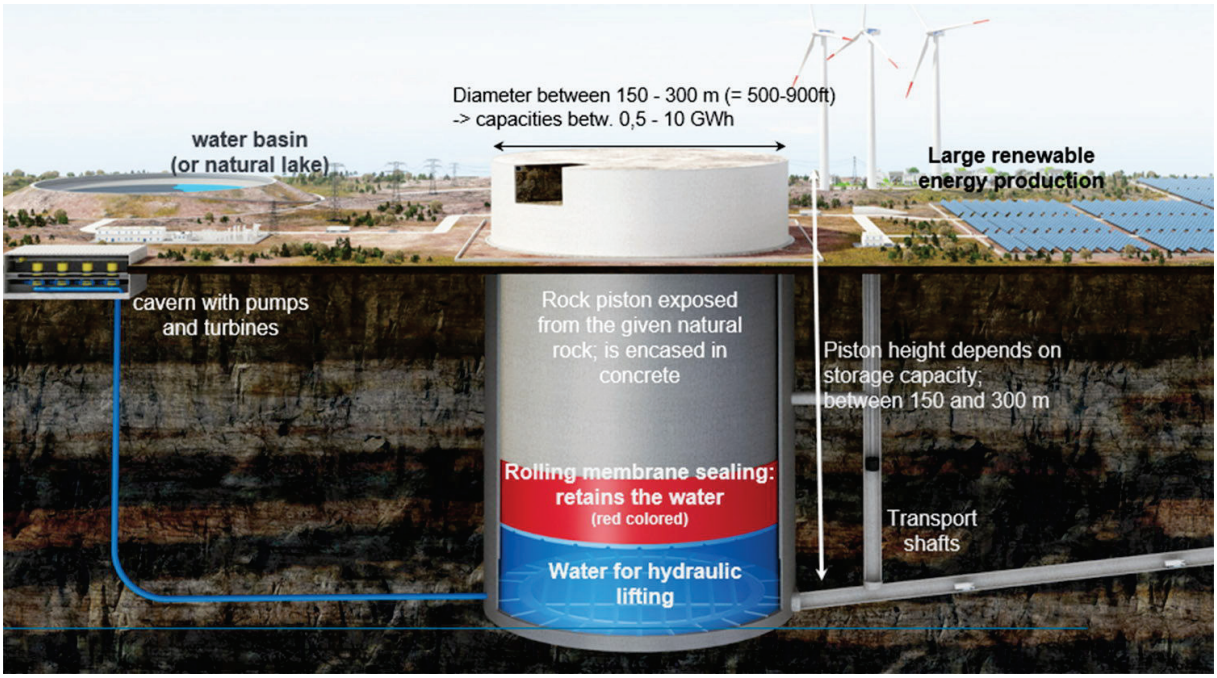

Figure 3: Technology of Gravity Storage (Gravity Storage, 2024)

Gravity Power uses a similar concept, with the only difference being that it operates as a closed-loop system (Figure 4). The water is pumped from above the piston below it to store energy, and the reverse happens to generate electrical energy. (Gravity Power, n.d.)

An overview of the different principles of SGES is displayed by Figure 5.

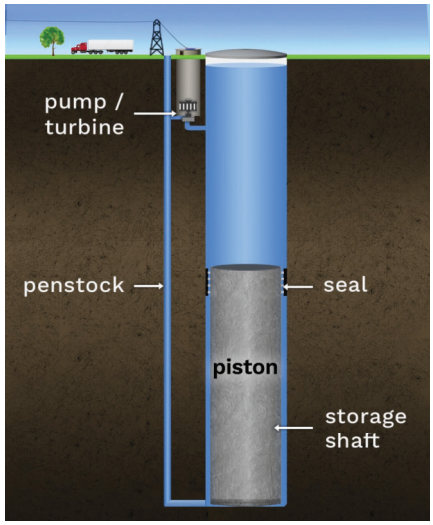

Figure 4: Technology of Gravity Power (Gravity Power, n.d.)

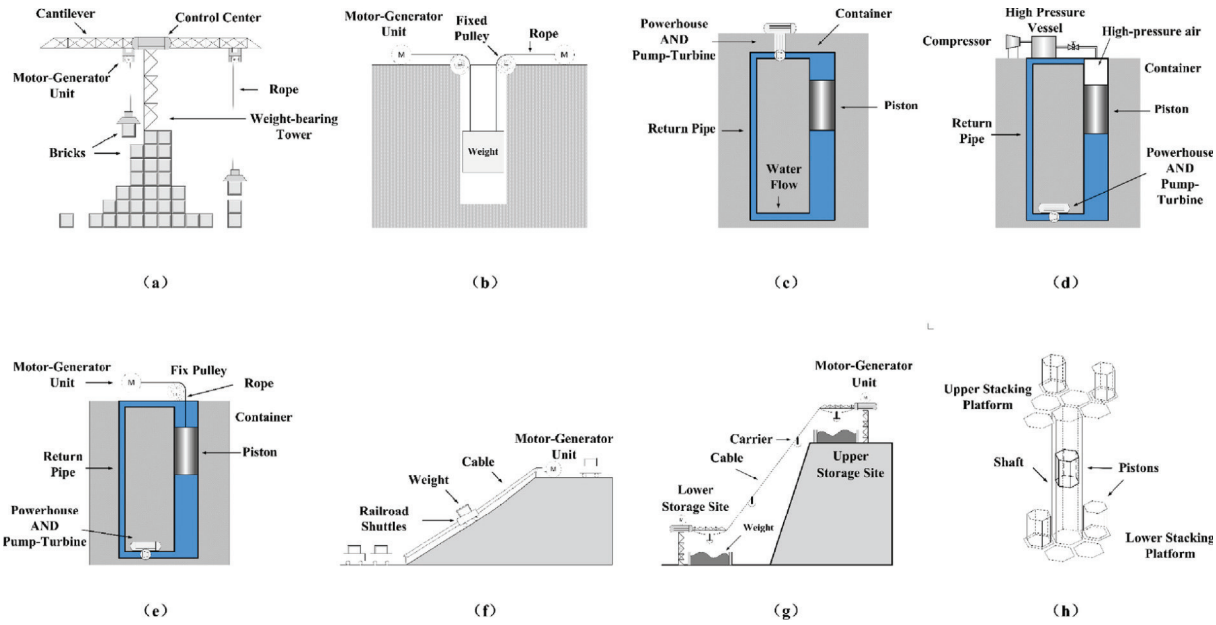

Figure 5: An overview of the different SGES technologies (Tong, Lu, Sun, et al., 2022, p. 929)

2.1.2 Pumped Hydropower Energy Storage (PHES)

A technology that is closely related to SGES is pumped hydropower energy storage. It is widespread and plays a major role in current energy storage (Schoenfisch & Dasgupta, 2023). If there is an oversupply of electricity, PHES systems pump water from the lower basin to the

upper basin with the help of electrical energy. On the contrary, if electricity is needed, the water flows down again, and a turbine generates electrical energy. (Zahoransky et al., 2019, p. 529)

2.1.3 Other Energy Storage Technologies

Another widespread storage technology is lithium-ion batteries. They work like normal batteries with an anode and a cathode that store the lithium. The positively charged lithium ions are transported through the separator between the cathode and the anode. The electrons cannot flow through the battery due to the separator. Hence, the movement of the lithium ions leads to a current flowing through the connected device during discharging. When the battery is charging, the lithium ions are moved back. (U.S. Department of Energy, 2023)

The flow batteries differ from conventional batteries in two main points: The reaction does not occur between the electrolyte and the electrode but between the two electrolytes. Thus, there is no loss in electroactive substance. Furthermore, the electrolytes are stored in external tanks, which require a circulation and a control system. These batteries are distinguished by the chemistry of their electrolytes, an example being the vanadium redox flow battery. (Blanc, 2009, pp. 22-23)

An energy storage technology that is considered to have potential for the storage of electrical energy over weeks and years is hydrogen. It can be gained by electrolysis of water with electricity. Then it is stored in tanks, and finally, fuel cells can be used to produce electricity again. (Zahoransky et al., 2019, p. 545)

2.2 Fundamental Concepts

In this chapter the fundamental concepts necessary to understand this paper are explained (Urone et al., 2022, pp. 153-154, 198-199, 203, 270, 275, 278, 293, 296, 408, 873-874). First of all, it is important to note that energy is always conserved. It can change its form, and it might be transferred from one system to another, but the total energy always remains the same. Different types of energy are listed below.

To get the potential energy, the gravitational force is needed. This is the force accelerating a

falling object with mass m. It is also called weight w, the formula of which is as follows:

$$w = m \cdot g\,, \tag{1}$$

where g is the gravitational acceleration on Earth, which amounts to 9.81 $\frac{\mathrm{m}}{\mathrm{s}^2}$ (Wetzel, 2019, p. 6).

The work done against the gravitational force means the work done when lifting an object with mass m through a height h. If the object is lifted straight upwards with a constant speed, the force needed to lift the object equals the weight. The formula to calculate the work done against the gravitational force is:

$$W = m \cdot g \cdot h \tag{2}$$

This is the gravitational potential energy (PE_g) put into an object-Earth system.

In terms of kinetic energy, there are two types. The translational kinetic energy is the energy of a translationally moving object with a mass m at a speed v:

$$KE_{\text{trans}} = \frac{1}{2} \cdot m \cdot v^2 \tag{3}$$

The rotational kinetic energy describes the energy of a rotating object with a moment of inertia I and an angular velocity ω:

$$KE_{\text{rot}} = \frac{1}{2} \cdot I \cdot \omega^2 \tag{4}$$

Considering the work done against friction, it is relevant to know that friction occurs when two surfaces are in contact and there is relative motion. The friction force opposes this motion. In a static situation there is static friction. When an object is moving, it is affected by kinetic friction, the magnitude f_{k} of which is calculated as demonstrated below:

$$f_{\mathrm{k}} = \mu_{\mathrm{k}} \cdot N\,, \tag{5}$$

where μ_{k} is the coefficient of kinetic friction, and N represents the magnitude of the normal force.

On a horizontal surface the normal force has the same magnitude as the weight. Due to the definition of work and weight, the work done against friction W_{fr} is defined by the following formula:

$$W_{\text{fr}} = \mu_{\text{k}} \cdot m \cdot g \cdot d \tag{6}$$

Moving on to the electrical energy, the relationship of energy E and power P depends on time t and is shown below:

$$E = P \cdot t \tag{7}$$

The electrical power P is defined by current I, voltage ΔV, and resistance R with the following formula:

$$P = I \cdot \Delta V = \frac{(\Delta V)^2}{R} = I^2 \cdot R \tag{8}$$

Even though the total energy is conserved during an energy conversion process, the output of useful energy or work W_{out} is smaller than the energy input E_{in}. The definition of the efficiency η is:

$$\eta = \frac{W_{\text{out}}}{E_{\text{in}}} \tag{9}$$

The product of the efficiencies of the different subsystems gives the efficiency of the whole process (The Pennsylvania State University, 2023).

2.2.1 DC Motor and Generator

One of the essential components of the SGES model is the DC motor. It converts electrical power P_{in} into mechanical power P_{out}. The total power loss P_{loss} during the conversion consists of frictional and copper losses, losses due to heat rise, and, if the DC motor is not coreless, there are iron losses. Therefore, P_{in} is defined as follows:

$$P_{\text{in}} = P_{\text{out}} + P_{\text{loss}} \tag{10}$$

The mechanical power of a DC motor can be calculated with the following formula:

$$P_{\text{out}} = M \cdot \omega_{\text{rad}} = M \cdot n \cdot \frac{2\pi}{60} \tag{11}$$

Where:

- P is the power in W
- M is the torque in Nm
- ω_{rad} is the angular velocity in $\frac{\text{rad}}{\text{s}}$
- n is the speed in min^{-1}

(Faulhaber, n.d.)

Brushed DC motors can operate as DC generators. The moving winding segment causes the induction of a sinusoidal voltage. The brushes turn the induced voltage into a DC voltage at the terminals. The voltage generated is proportional to the shaft speed:

$$\Delta V_{\text{ind}} = \frac{n}{k_{\text{n}}} = k_{\text{g}} \cdot n \tag{12}$$

Where:

- ΔV_{ind} is the induced voltage in V
- n is the speed in rpm
- k_{n} is the speed constant of the motor in $\frac{\text{rpm}}{\text{V}}$
- k_{g} is the generator constant of the motor in $\frac{\text{V}}{\text{rpm}}$

If a generator is unloaded, ΔV_{ind} is obtained at its terminals. When the terminal is loaded with a current, the terminal voltage ΔV_{t} is reduced by the voltage drop at the motor resistance R_{mot} for a given load current I_{L}:

$$\Delta V_t = \frac{n}{k_{\text{n}}} - R_{\text{mot}} \cdot I_{\text{L}} \tag{13}$$

The resistance of the motor is defined as follows:

$$R_{\text{mot}} = \frac{\Delta(\Delta V_{\text{t}})}{\Delta I_{\text{L}}} \tag{14}$$

(Kafader, 2019)

2.2.2 Gear Unit

Another key component of the SGES model is the gear unit. In gearboxes, the torque and the speed are converted by gears of different sizes. The transmission ratio describes the change of speed between a driving and a driven wheel:

$$i = \frac{n_1}{n_2} \tag{15}$$

Where:

- i is the transmission ratio
- n_1 is the rotational speed of the driving wheel
- n_2 is the rotational speed of the driven wheel

The transmission ratio of a gear stage[1] is determined as follows:

$$i = \frac{z_2}{z_1} = \frac{d_2}{d_1} \tag{16}$$

Where:

- z is the number of teeth
- d is the operating pitch circle diameter

The total transmission ratio over all gear stages is calculated like this:

$$i_t = i_1 \cdot i_2 \cdot i_3 \cdot \ldots \tag{17}$$

[1] two gears meshing together

The tooth flanks of the driving gear press at the pitch circle on the tooth flanks of the driven gear with a certain force. Due to the different diameters of the gears, the torque is converted in this way:

$$M_2 = M_1 \cdot i, \tag{18}$$

where M is the torque.

This formula only applies if the power is constant throughout the gearbox. In practice, there is always a loss due to friction. This is taken into account in the following formula:

$$M_2 = M_1 \cdot i \cdot \eta_\mathrm{g}, \tag{19}$$

where η_g is the gear efficiency. (Höfler, 2018)

2.2.3 Photovoltaic (PV) Cell

The photovoltaic cell, also called a solar cell, is another important component of the SGES model. It converts sunlight into electricity, and it is the basic building block for a PV system. Sunlight consists of photons that contain energy. The photons can be reflected by the PV cell, pass through it, or they are absorbed by the semiconductor material of which the PV cell is made. When enough solar energy is absorbed, electrons are detached from the material's atoms. The electrons migrate to the surface of the PV cell due to special treatment during manufacturing. The difference of electrical charge between the front and the back results in a voltage. The electricity generated by PV cells is direct current (DC) electricity. By 2024, the efficiency of PV cells to convert from sunlight to electricity is around 25 %. (U.S. Energy Information Administration, 2024)

3 Materials and Methods

This chapter lists the used materials and shows the development of the self-constructed SGES model. It explains also how the results were measured, it shows the research methodology, and it lists the criteria utilised for the comparative analysis.

3.1 Materials Utilised

Most of the used material had been bought: a DC motor with suitable screws, a propeller hub, two servo motors, seven ball bearings, an LED spotlight (8250 lm), four solar cells, an Arduino UNO with a 9 V-battery and a corresponding connection cable, a bistable relay, a breadboard, jumper cables, normal cables, and two buttons with two 1 kΩ resistors. Other components were provided by the school: four white LEDs and four 100 Ω resistors. Additional utilised materials were cables to connect the spotlight to the wall socket, a connection cable to program the Arduino, and two multimeters. The model was built with the help of wood slats and wood plates as well as 3D-printed parts. Some of these materials are more closely described in the following subchapters.

3.1.1 PV Cell

The used mini solar cell panel has the following characteristics:

- Solar cell type: polycrystalline
- Maximum power: 0.39 W
- Rated voltage (V_{mp}): 6 V
- Rated current (I_{mp}): 0.065 A
- Open circuit voltage (V_{oc}): 7.13 V
- Short circuit current (I_{sc}): 0.081 A
- Dimension: 60 x 60 mm

(Conrad Electronic, n.d.-a)

3.1.2 DC Motor

Furthermore, the utilised DC motor possesses the following characteristics:

- Voltage range: 0.18 V - 6 V
- Rated voltage: 2 V
- Rated load: 3 g – cm

At rated voltage and rated load, the motor has these specifications:

- Rated load current: 0.07 A
- Rated load speed: 1700 rpm

And at rated voltage and no load, these characteristics are valid:

- No load current: 0.018 A
- No load speed: 2300 rpm

(Conrad Electronic, n.d.-c; Shenzhen Hua Chuang Sheng Motor Co., 2014, pp. 1, 3)

3.1.3 Servo Motor

Moreover, the employed servo motors of type HD-1800A possess the following specifications:

- Stall torque at locked (at 4.8 V): 1.0 kg – cm
- Operation speed at no load (at 4.8 V): 0.11 $\frac{s}{60^\circ}$

(Power HD, n.d.)

3.1.4 Bistable Relay

In addition, the used bistable relay of the type G6AK-274P-ST-US 5 VDC possesses the following characteristics:

- Rated voltage: 5 V
- Rated current: 0.036 A

- Set and reset time: approx. 2.5 ms, max. 5 ms

(Conrad Electronic, n.d.-b; Omron, n.d., pp. 111, 113)

3.2 Development of the Model

Using these materials, a model of a solid gravity energy storage system could be developed. The basic idea to build this model was to have a mass[2], pulled vertically up by solar cells, and when the mass goes down, it makes LEDs shine. It is therefore most similar to type b in Figure 5.

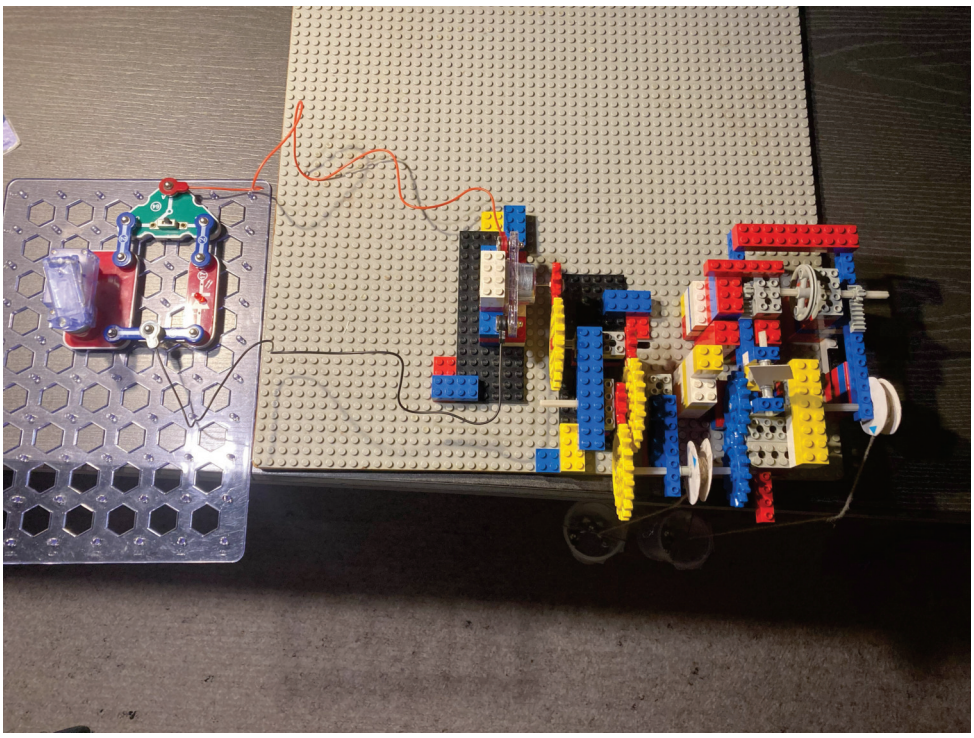

Figure 6: Model with clamping blocks

Initial ideas for the model emerged by utilising plastic clamping blocks, one LED, and a hand-operated power source (Figure 6). The key findings indicated that a gear unit is necessary between the lifting axis and the motor axis. Another idea involved adding another mass[3] that could slow down the main mass by going up and then release the potential energy gained by

[2]called "main mass"
[3]called "assisting mass"

pulling the main mass up. Additionally, it could accelerate the main mass at the top. How exactly this could be useful will be examined in this paper too.

Then calculations were conducted to gain a better understanding of the physics behind the model, and therefore to be able to estimate the correct sizes for the parts of the model. For this purpose, the formulas from Section 2.2 were utilised. In the case of the gear, the choice settled on a radius of 0.05 m and 0.005 m for the two gear wheels and two translations for the gear unit. The spool used to wind up the rope on which the main mass hangs should be 23.2 mm in diameter.

The next step was to find fitting components. The motor had to be a brushed DC motor (see Sec. 2.2.1) that would start to work already with a low power supply. Additionally, the maximal voltage of the solar cells and the motor had to fit, such that the motor did not break.

The construction of the model started with the gear unit and its frame. The gear wheels were constructed using a costum feature in Onshape (Neil, 2023). The other parts were also designed utilising Onshape and then printed on the 3D printer. The small gear wheel was attached at the motor axis with a propeller hub. The rest of the gear unit was first only fixed in a wood rod (Figure 7). Because it had too much friction, ball bearings were used. To fix them better, the frame was also made with the 3D printer (Figure 8).

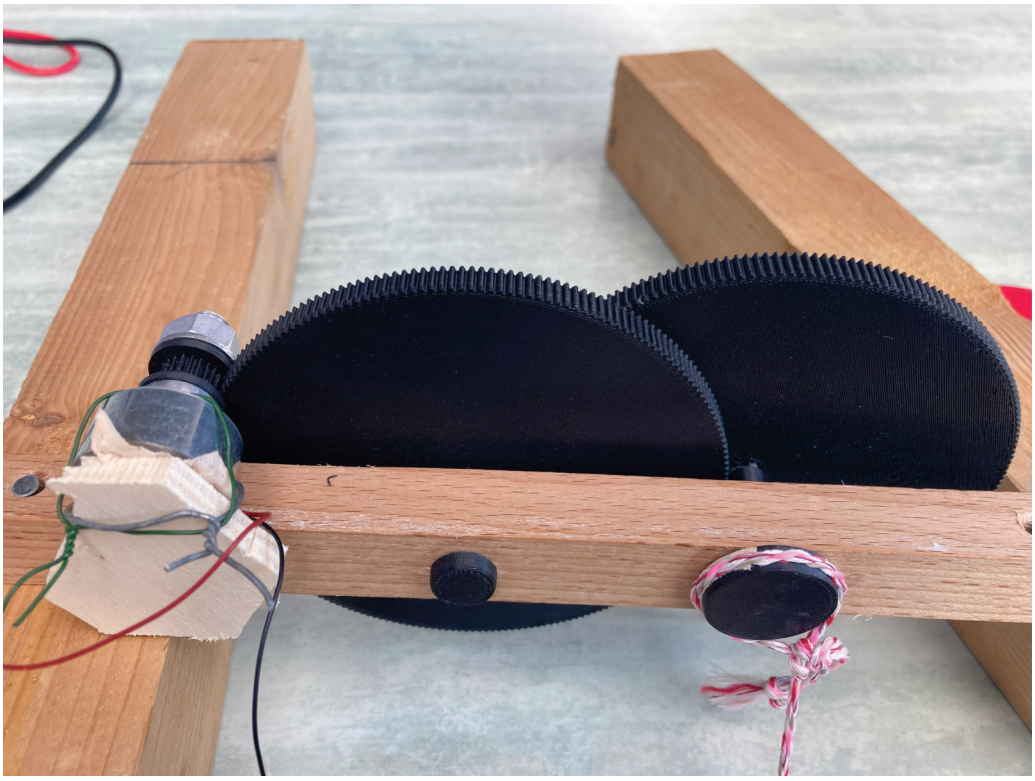

Figure 7: First prototype

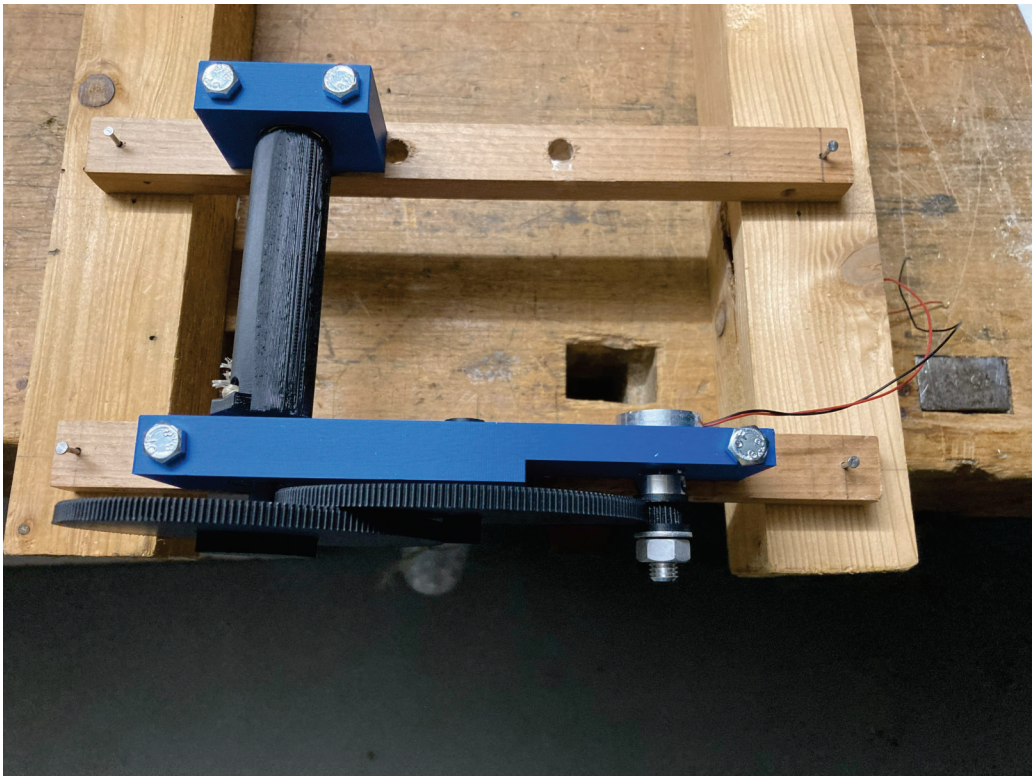

Figure 8: Second prototype

The gear teeth were too little to mesh with each other. Consequently, the teeth were enlarged, and the new radii of the gear wheels were 0.065 m and 0.0065 m. An attempt was made to use a spool with a smaller diameter in order to use a larger mass and therefore store more energy while maintaining the same power output. Different spools were tested. If a too small diameter was used, the spool bent, and that made the gear wheel tilt. Finally, a spool with a diameter of 13 mm was used. The final main mass used amounted to 0.987 kg.

The connection of the gear wheel and the spool was made with a cross at the spool, which was put into a cross hole in the gear wheel. A significant issue was that this cross often broke. To solve this problem, the cross was printed as a part itself with 100 % infill, and the print was layered orthogonally to the force acting on it. Before that, the layers had been vertically orientated and could break more easily. After this change, the layers were horizontal. Both the spool and the gear wheel were designed with a cross hole. Another difficulty existed because the gear wheels swivelled back and forth while turning. To overcome that, the gear wheels were stabilised with a ball bearing on the other side too (Figure 9).

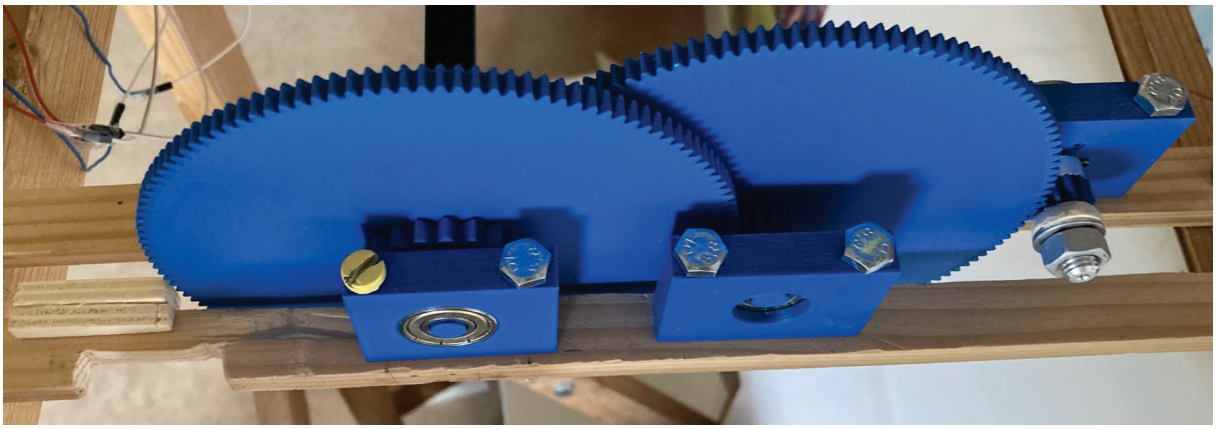

Figure 9: Fixation of the gear wheels

A framework with wooden slats was erected to get enough height over which the mass can move up and down (Figure 18). The gear unit was fixed on the top of it.

The first idea suggested that another mass was needed to overcome the static friction for the main mass at the beginning. It needed to be pulled up together with the main mass, then it would be disconnected and blocked by a brake. When the main mass had to start going down, the assisting mass should connect, and the brake would be released. By moving downwards,

it needed to accelerate the main mass. After the acceleration, it would be disconnected again. After some tests, it became clear that the main mass accelerates without support. However, it was examined if the assisting mass was efficiently helpful to accelerate faster. This would lead to a constant power output sooner as well as earlier shining LEDs. The assisting mass should also be a support to stop the main mass. It would be connected to the main mass and should slow it down, whereby the assisting mass would move upwards. Afterwards, the assisting mass had to move down again to accelerate the main mass. Therefore, it should preserve energy as potential energy of the assisting mass.

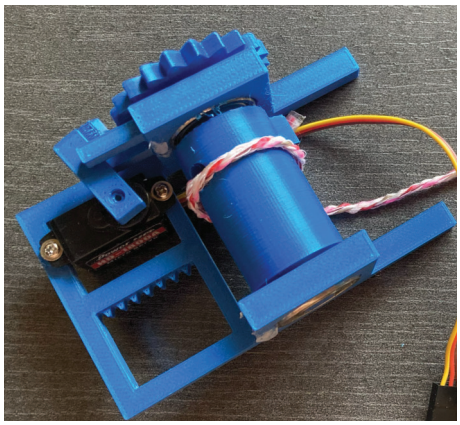

Figure 10: First dynamic spool frame

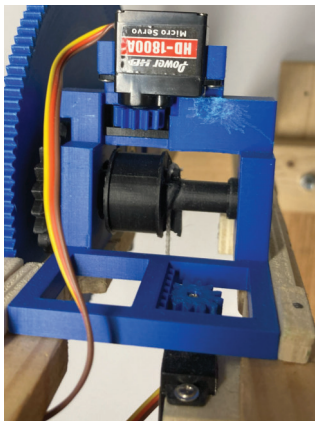

Figure 11: Second dynamic spool frame

To connect the spool of the assisting mass, a gear wheel was used. It has sharp teeth, such that it can connect without problems. This gear wheel is attached to the spool that holds the assisting mass. This spool is held by a frame that can move back and forth[4].

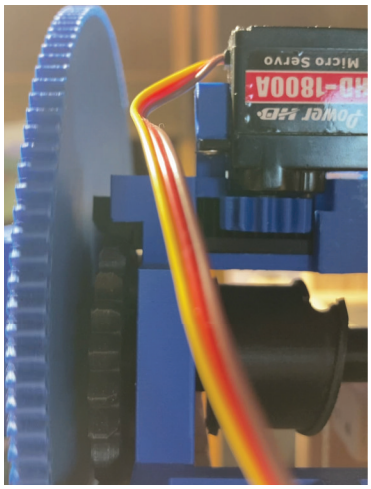

Figure 12: Brake

The brake was first designed like shown in Figure 10. However, the brake slid backwards when it was connected, and there was too much mass hanging on the spools. Therefore, a second, more stable design replaced it (Figure 12). In this design, both the brake and the gear wheel teeth were sharpened on the side facing each other, such that they connect more easily.

The spool was first chosen the same size as the main spool (diameter: 13 mm), and the mass

[4]called "dynamic spool frame"

was adapted when necessary. However, for the deceleration at the bottom, a larger torque was required. Whereas the acceleration at the top needed a smaller torque due to the fact that the power of the solar cells was not enough to pull up the main mass as well as the assisting mass with a large torque. For that reason, and because the assisting mass cannot change its mass, it became clear that for the acceleration at the top, a smaller diameter was needed than for the deceleration at the bottom. Therefore, for the acceleration at the top a diameter of 9 mm was chosen and 23.2 mm for the deceleration at the bottom. A special spool was designed to unite these two diameters in one spool (Figure 11). Depending on the direction in which the spool turned, the rope was wound around a spool with a different radius. Hence, the torque was different. The utilised assisting mass had a mass of 0.469 kg.

A model house of wood (Figure 16) was built to install four solar cells on top of it and four LEDs inside, each of which had a 100 Ω resistor in series. The LEDs and the solar cells were connected to the motor.

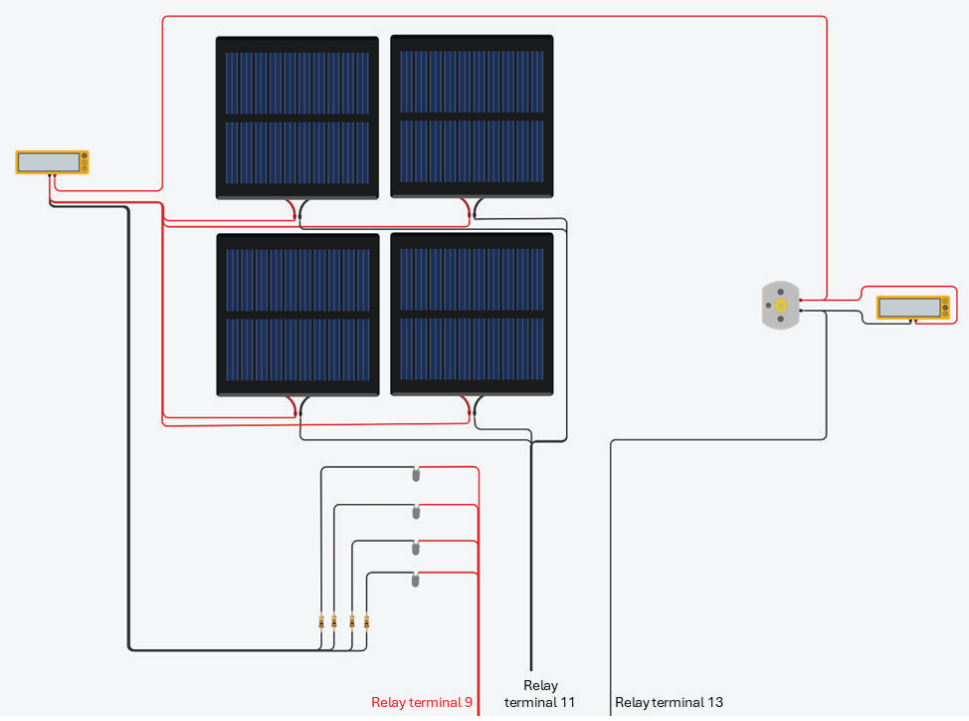

Figure 13: Circuit diagram of the solar cells, the LEDs, and the motor (created using Tinkercad (Autodesk, 2024))

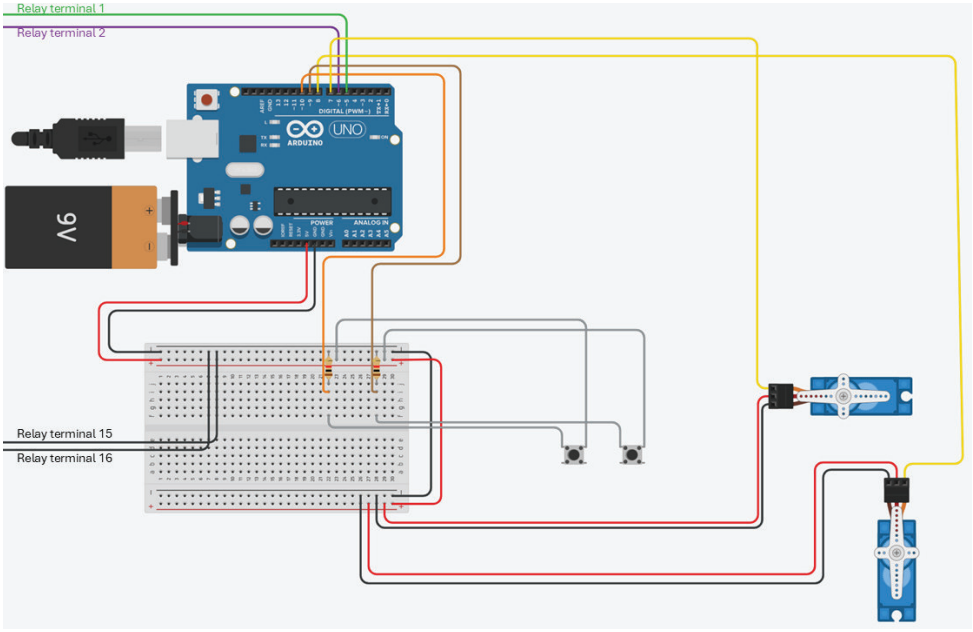

Figure 14: Circuit diagram of the electronic control unit (created using Tinkercad (Autodesk, 2024))

To make the model closer to real life, an electronic control unit was utilised (Figure 14). An Arduino UNO served as a microcontroller. It was programmed with a program called Arduino IDE. A bistable relay (Figure 15) operated as a switch between the solar cells and the LEDs (Figure 13). Two servo motors were employed for the movements of the dynamic spool frame and the brake. To control the actions, buttons were used. The resistors that were needed to utilise the buttons had a resistance of 1 kΩ.

The house and the electronic control unit were installed on a wooden board next to the mechanical components. Above the house, a spotlight was screwed on, as a constant sun simulation for the solar cells (Figure 16).

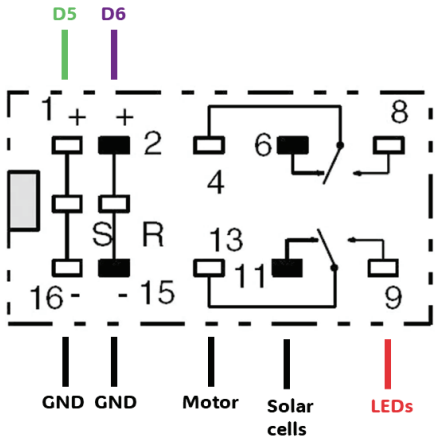

Figure 15: Ports of the bistable relay (Conrad Electronic, n.d.-b) with added labelling

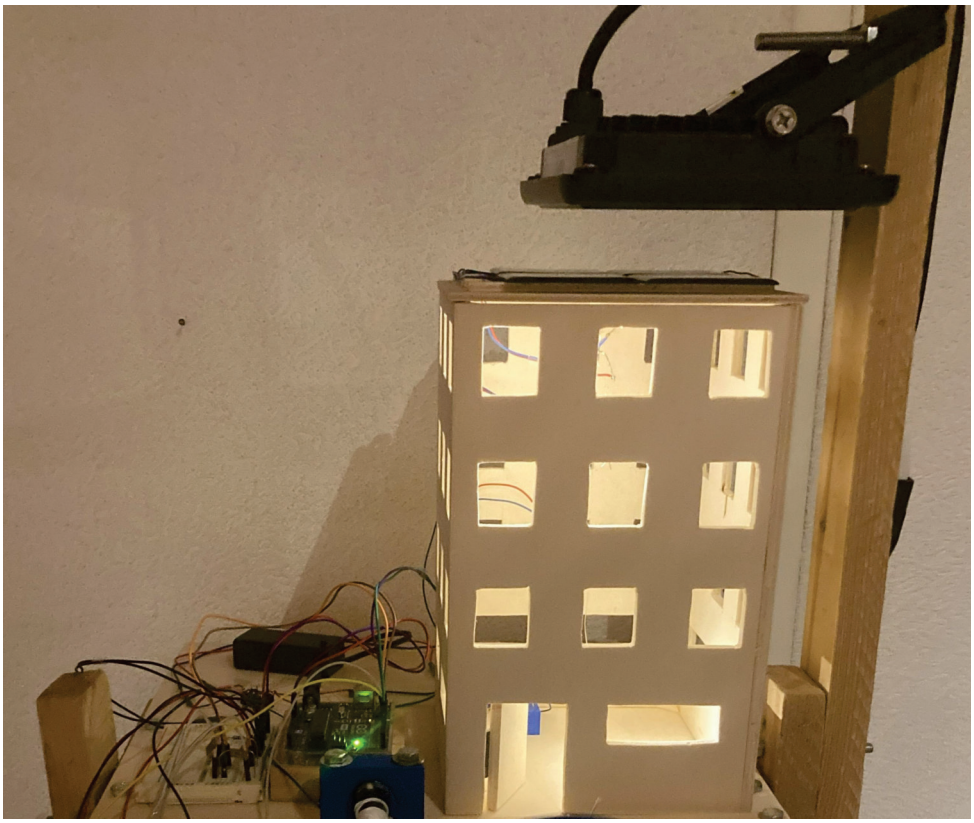

Figure 16: Electronic control unit and model house

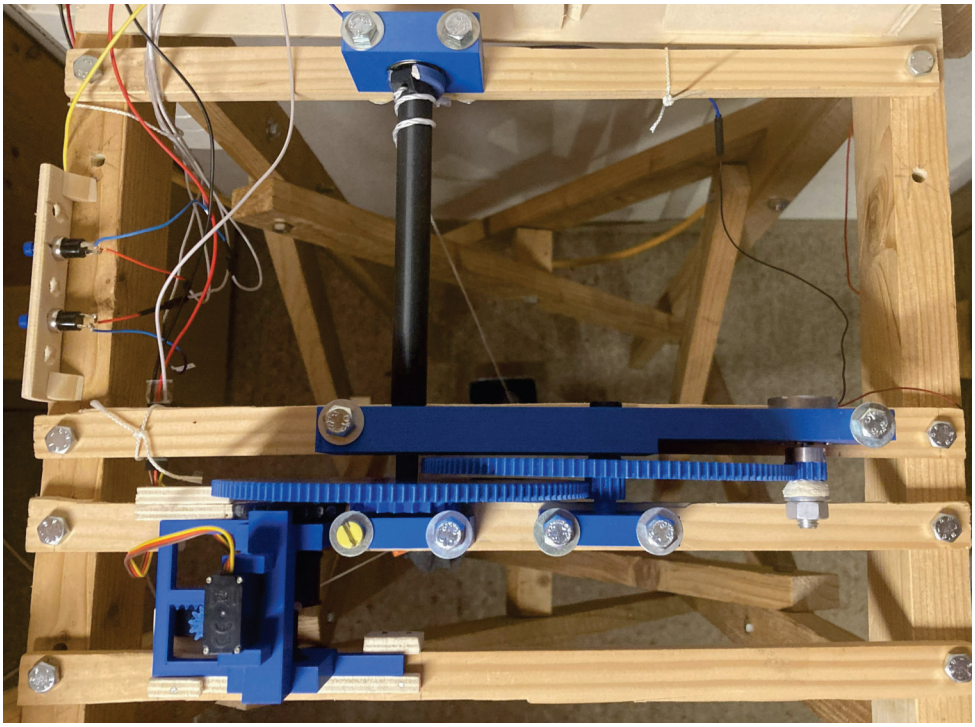

Figure 17: Mechanical unit

Figure 17 shows the final result of the gear unit. There, the motor is at the right, and the spool to wind up the rope of the main mass is at the left of the gear unit. The gear wheel of the main mass has another gear wheel attached firmly to it, which can be connected to the gear wheel on the dynamic spool frame. These two gear wheels have the same number of teeth. The dynamic spool frame holds the spool of the assisting mass. To connect and disconnect the assisting mass, it is moved forward and back by a servo motor with a gear wheel that is connected to a gear rack. The same principle is used to move the brake.

The final process is as follows: While the main mass moves down, the motor is connected to the electric circuit with the LEDs. The process to make the main mass move up again at the lowest point,[5] can be introduced by the corresponding button. It begins by connecting the dynamic spool frame to the gear unit. The assisting mass slows the main mass down by winding up around the thick part of the spool. After it is slowed down to the point where the LEDs stop shining, and therefore the main mass is nearly stopped, the relay switches to the electric circuit with the solar cells. The assisting mass supports the upward motion by moving down. Then, it is pulled up a bit by winding around the thin part of the spool to support the start at the top later. The brake brakes the gear wheel of the assisting mass, and the dynamic spool frame disconnects. At the topmost point, another button initiates the process of moving downwards again.[6] The relay switches to the electric circuit with the LEDs, the assisting mass connects, and the brake releases. The assisting mass accelerates the main mass additionally before it detaches again.

[5] called "deceleration at the bottom"
[6] called "acceleration at the top"

3.3 Measurement Techniques

Figure 18: Measurement setup

Figure 19: Measurement in Tracker

To analyse the developed model, two videos were taken. One which used the assisting mass to accelerate at the topmost as well as to brake at the lowest point (code for the measurement with an assisting mass see Appendix B) and another without the utilisation of the assisting mass (code for the measurement without an assisting mass see Appendix B). To measure the motion, the program Tracker was used. To track the mass, it was necessary to indicate a reference length (Figure 19) and to mark the mass with a cube in an outstanding colour. To help Tracker keep track of the mass, the background had been made plain white. To ensure that the coloured cube is visible the whole time, the front wooden slat cross of the framework had to be removed.

To determine the voltage and the current, two multimeters were connected to the electric circuit (Figure 13). The voltage drop over the motor was recorded, and the current was measured next to the motor. The measured figures were read from the videos. During all measurements, only a 100 Ω resistor was connected to the DC motor instead of the LEDs due to their special behaviour. However, they were intended to demonstrate the model. Therefore, the final programming code (see Appendix B) uses other delay times during braking, among other adjustments. The whole setup is shown in Figure 18.

The numerical results were analysed with Excel. It should be noted that only the motion over the vertical axis was considered for the position data because the horizontal movement is not important. The relevant data is included in Appendix A. This data is partly rounded. Therefore, the results in this paper might slightly differ from the results calculated directly with these data.

To determine the energy consumption of the electronic control unit, the voltmeter and the ammeter were connected to the battery that supplies the Arduino with power (Figure 20). The ammeter was attached next to the battery (red cables), and the voltmeter was connected to both poles of the battery (a blue and a red cable). The gained data was also analysed with Excel.

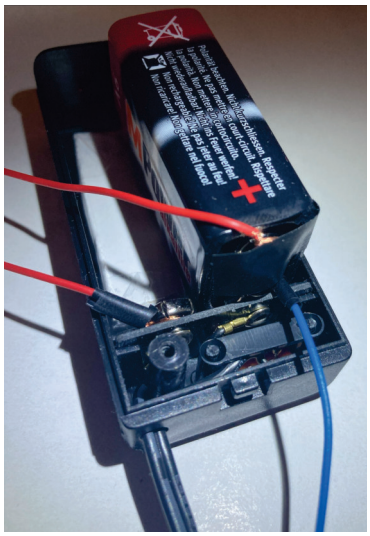

Figure 20: Battery connected to measurement devices

3.4 Research Methodology

To enrich the practical work, research was conducted, for which mainly Google and BASE were used. The search terms included, for instance, "gravity as energy storage", "solid gravity energy storage system", and "energy storage technologies compared". To find data about Switzerland, German terms were utilised, such as "Strombedarf Schweiz in den letzten Jahren". Among the online sources, the paper also refers to the book Zahoransky Richard, 2019, Energietechnik, Springer Vieweg.

3.5 Criteria for the Comparative Analysis

The researched information about the different storage technologies was compared with the criteria that are followingly listed. Some general aspects assessed were the maturity of the technology, how economically profitable it is, and, in particular, the levelized cost of electricity (LCOE). The LCOE of an energy storage system is the ratio between what it costs during its lifetime and the total amount of electricity it produces during the same time (Tong, Lu, Chen, et al., 2022, p. 23). As the currency is ¥, it is converted by using the fact that CNY 100 corresponded to CHF 14.6573 at the time of the publication of the figures (ESTV, n.d.). One of the outlined technical specifications was the round-trip efficiency, which is the ratio between energy output and energy input over a complete charge and discharge cycle (Arangarajan et al., 2015, p. 5). Another relevant indicator was the energy-to-power ratio, which is the ratio between the installed energy capacity and the installed power (Sauer et al., 2012, p. 10). Furthermore, the self-discharge rate was regarded, which is the loss of energy of an energy storage system in charge over a longer period without use (Arangarajan et al., 2015, p. 7). Additional evaluated characteristics were the energy density, the power density, and the depth discharge limit. Also considered were the response time, the lifetime, and the degradation of components of the storage technology with a following performance loss. In addition, the topographical adaptability and the sustainability were assessed.

4 Results

In this section the results of the analytical measurements of the SGES model are shown. Furthermore, it was approximately calculated how the figures would look if the model had a realistic size.

4.1 Outcomes of the SGES Model Measurements

The analysis of the two videos taken (see Sec. 3.3) resulted in the following diagrams. The outcomes of the measurement where no assisting mass was used are shown in Figure 21 and in Figure 22. In this procedure, the main mass was moving upwards at second 0. After approximately 32 seconds, the relay switched to the electric circuit with the resistor, and the main mass started to move downwards. Around second 52, the relay switched back to the circuit with the solar cells, causing the main mass to move up again.

Figure 23, Figure 24, and Figure 25 show the results of the measurement with an assisting mass. This process started with the relay switching to the electric circuit with the solar cells shortly before second 1. Around second 2, the assisting mass changed its downward motion to being pulled upwards. Then the dynamic spool frame detached around second 6. At this time, the main mass was moving upwards. Approximately at second 37, the relay switched to the circuit with the resistor, and the dynamic spool frame attached to accelerate the main mass. Roughly at the 39th second, the dynamic spool frame detached again. Then the main mass was moving downwards. Shortly before the 60th second, the dynamic spool frame attached again to decelerate the main mass. Approximately at second 63, the relay switched again to the circuit with the solar cells. Around second 64, the assisting mass changed from moving down to being pulled up, and the dynamic spool frame detached approximately at second 68. At this point, the main mass was in upward motion again.

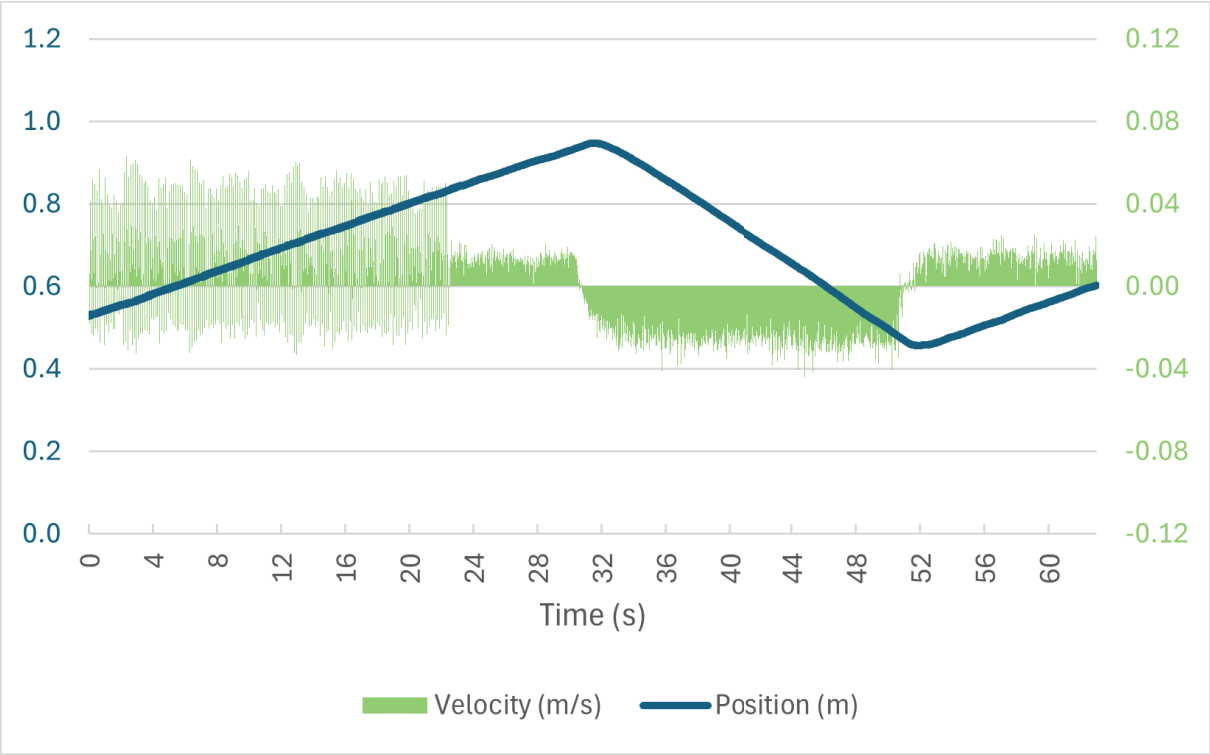

Figure 21: Motion of the main mass in the operation without an assisting mass

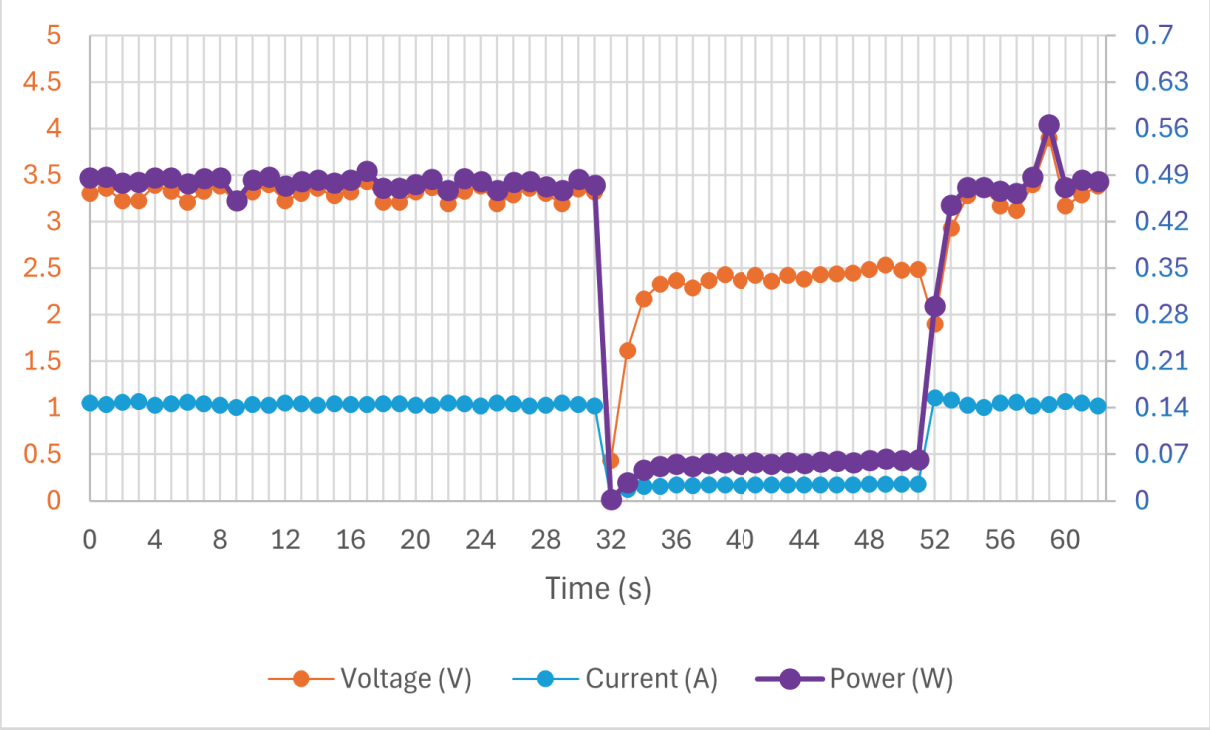

Figure 22: Electrical data during the operation without an assisting mass

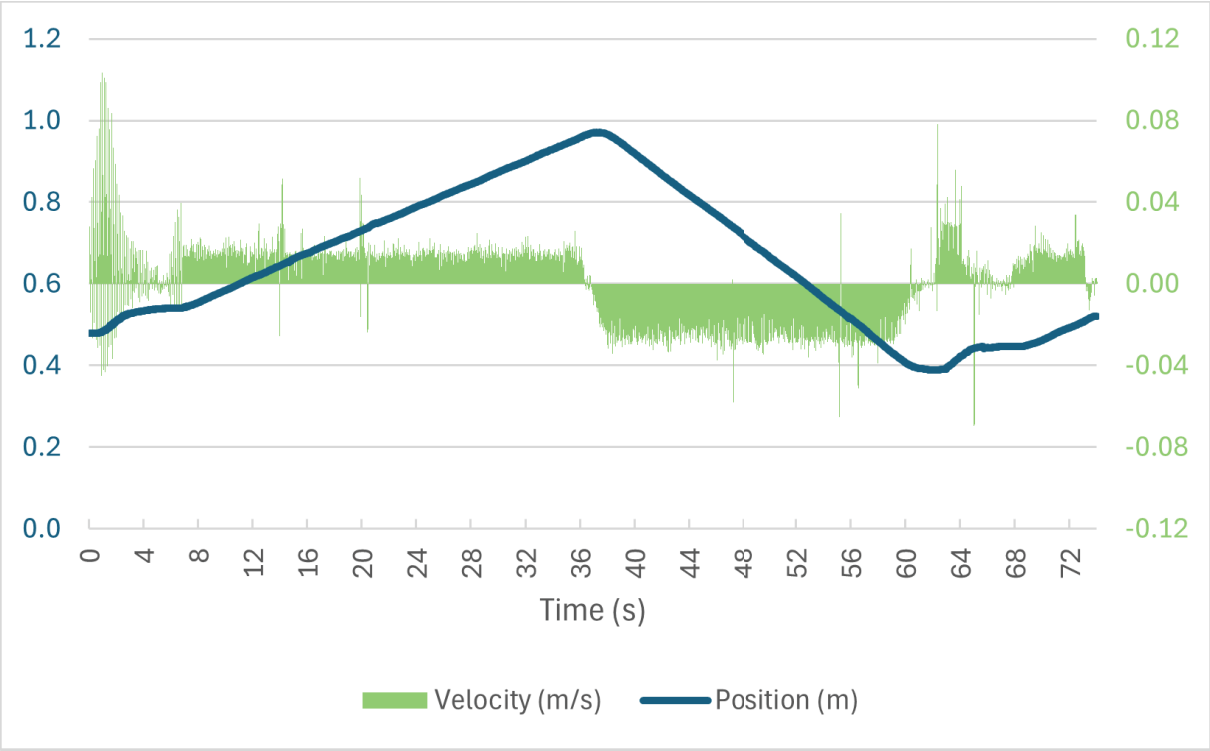

Figure 23: Motion of the main mass in the operation with an assisting mass

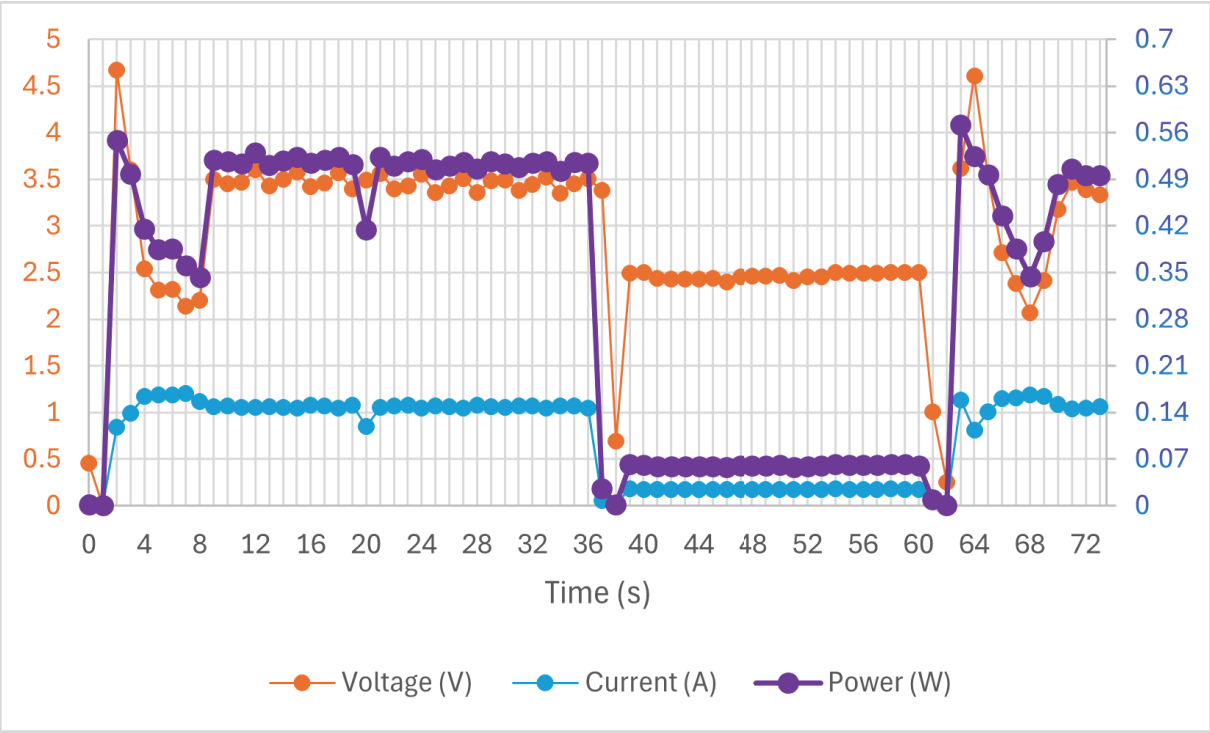

Figure 24: Electrical data during the operation with an assisting mass

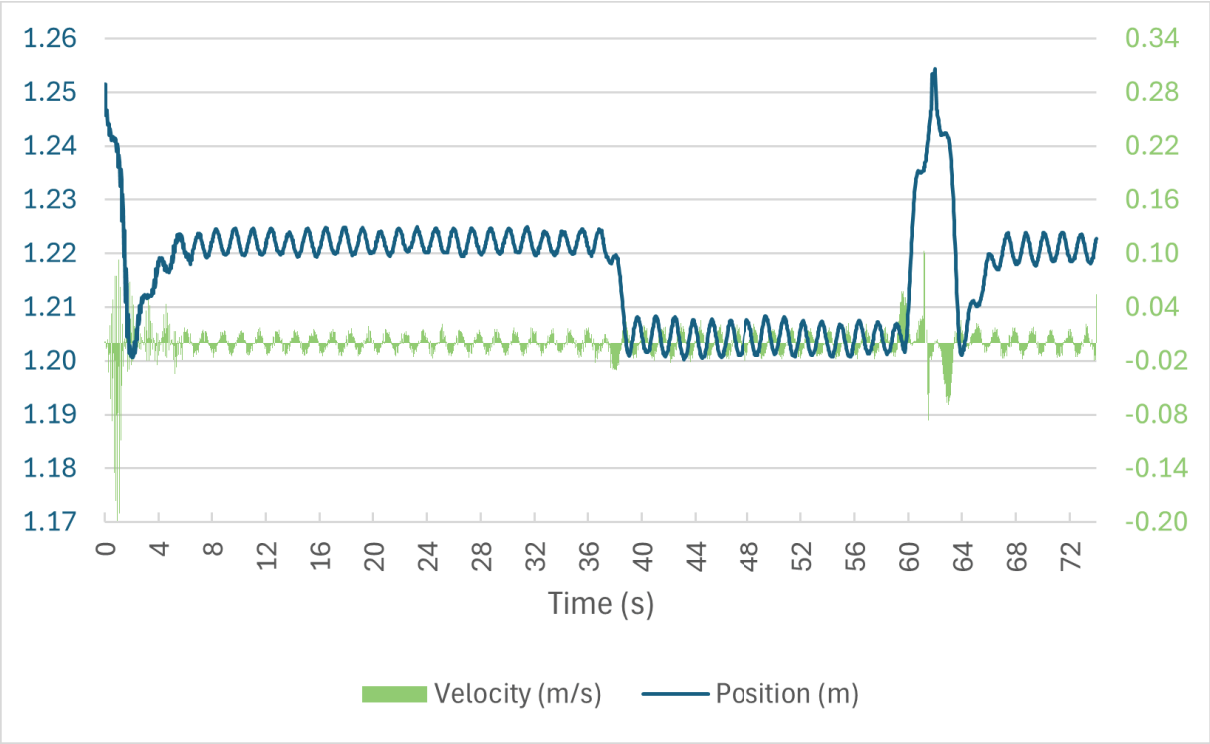

Figure 25: Motion of the assisting mass in the operation with an assisting mass

4.1.1 Efficiency

The efficiency was calculated for the measurements with and without an assisting mass. In order to calculate the efficiency, certain time frames of the upward motion and the downward motion in which the main mass moves over the same length were considered. In this analysis, 0.1 m were taken. Two types of efficiency can be determined. One is the round-trip efficiency $\eta_{\text{round-trip}}$ from the input of electrical energy to the output of electrical energy. The other efficiencies look separately at the upward and the downward motion. η_{upwards} represents the efficiency of converting the electrical energy input into the potential energy output. $\eta_{\text{downwards}}$ denotes the efficiency of converting the potential energy input into the electrical energy output. The electrical input energy $E_{\text{el solar}}$ and the electrical output energy $E_{\text{el resistor}}$ were calculated by multiplying the time needed to pass these 0.1 m, which was taken from the Tracker data, and the power average during that time frame. The potential energy $E_{\text{mechanical}}$ was calculated with the formula in Equation (2) by using the mass of the main mass (0.987 kg) and the height

difference that is approximately 0.1 m. The round-trip efficiency was calculated as follows:

$$\eta_{\text{round-trip}} = \frac{E_{\text{el resistor}}}{E_{\text{el solar}}} \tag{20}$$

The efficiency during the upward motion was calculated by the ensuing formula:

$$\eta_{\text{upwards}} = \frac{E_{\text{mechanical}}}{E_{\text{el solar}}} \tag{21}$$

Whereas the efficiency for the downward motion could be determined by this formula:

$$\eta_{\text{downwards}} = \frac{E_{\text{el resistor}}}{E_{\text{mechanical}}} \tag{22}$$

The results for the measurement without an assisting mass are given below:

- $\eta_{\text{round-trip}} = 6.2\,\%$
- $\eta_{\text{upwards}} = 26.7\,\%$
- $\eta_{\text{downwards}} = 23.3\,\%$

For the measurement with an assisting mass, the results are as follows:

- $\eta_{\text{round-trip}} = 7.0\,\%$
- $\eta_{\text{upwards}} = 28.2\,\%$
- $\eta_{\text{downwards}} = 24.8\,\%$

4.1.2 Maximum Energy Storage Capacity

To calculate the maximum potential energy storage capacity $E_{\text{mechanical}}$ of the SGES model, the maximum height difference that the main mass can achieve was measured. If some margin to the top is left, an approximate value of 1.2 m is determined. With the mass of the main mass and the Equation (2), a maximum mechanical potential energy storage capacity of 11.62 J was determined. For the following two calculations, the efficiency data of the operation with an assisting mass was utilised (see Sec. 4.1.1). Firstly, the total electrical energy $E_{\text{el solar}}$ needed to

achieve this height could be calculated as follows:

$$E_{\text{el solar}} = \frac{E_{\text{mechanical}}}{\eta_{\text{upwards}}} = \frac{11.62\,\text{J}}{28.2\,\%} = 41.21\,\text{J} \tag{23}$$

Secondly, the maximum electrical energy output $E_{\text{el resistor}}$ of the SGES model was calculated with the ensuing formula:

$$E_{\text{el resistor}} = E_{\text{mechanical}} \cdot \eta_{\text{downwards}} = 11.62\,\text{J} \cdot 24.8\,\% = 2.88\,\text{J} \tag{24}$$

4.1.3 Acceleration at the Top

The assisting mass consumed additional energy generated by the solar cells when it was pulled up together with the main mass. But it also led to more electrical energy while it moved down. To compare the operation with and without an assisting mass, two different parts were important: In the interval where the assisting mass was pulled up together with the main mass, the energy $E_{\text{solar with}}$ was required. It was compared to a part of the upward motion during the operation without an assisting mass of the same length, which utilised the energy $E_{\text{solar without}}$. The second part considered was the interval in which the main mass was accelerated, from which again the same distances were taken. Additionally, it was paid attention to that in both measurements the main mass was fully accelerated. The gained energy in this part was $E_{\text{resistor without}}$ for the measurement without an assisting mass and $E_{\text{resistor with}}$ for the measurement with an assisting mass. The energy consumed or generated in these parts was calculated by taking the average power and multiplying it with the time passed. The time was taken from the Tracker data. The time intervals at which the power was measured varied, depending on whether it changed in a short period of time that led to insufficient data to show how it changed. The energy $E_{\text{surplus needed}}$ that the operation with an assisting mass additionally needed was calculated as follows:

$$E_{\text{surplus needed}} = E_{\text{solar with}} - E_{\text{solar without}} = 0.91\,\text{J} \tag{25}$$

With the help of the round-trip efficiency of the operation with an assisting mass (see Sec. 4.1.1), it is possible to calculate how much energy $E_{\text{potentially gained}}$ could be released from the

additionally needed electrical energy if it was used only to pull up the main mass. This was determined with the following calculation:

$$E_{\text{potentially gained}} = E_{\text{surplus needed}} \cdot \eta_{\text{round-trip}} = 0.06\,\text{J} \tag{26}$$

To calculate the energy $E_{\text{surplus gained}}$ that was additionally gained by using the assisting mass, the following formula was used:

$$E_{\text{surplus gained}} = E_{\text{resistor with}} - E_{\text{resistor without}} = 0.02\,\text{J} \tag{27}$$

An additional figure that could be calculated is the time it took to reach a constant power, which means the time t_{acc} needed to completely accelerate the main mass. To find this time, two time marks were important. Firstly, when the main mass started to move downwards at the top t_{start}, which is the first figure of the respective table. And secondly, the time when a nearly constant power was reached t_{end}. The conducted calculation was as follows:

$$t_{\text{acc}} = t_{\text{end}} - t_{\text{start}} \tag{28}$$

For the operation without an assisting mass, the acceleration lasted approximately 3.5 s (Table 18). Whereas the acceleration in the operation with an assisting mass required roughly 1.8 s (Table 16).

4.1.4 Deceleration at the Bottom

While the assisting mass was slowing down the main mass, less electrical energy was generated than without an assisting mass. However, the operation without an assisting mass consumed more electrical energy from the solar cells to decelerate and accelerate the main mass at the lowest point, while the assisting mass supported the acceleration of the main mass. To compare the effectiveness of this method, two parts were relevant. On the one hand, the energy output $E_{\text{resistor with}}$ of the interval from the point where the assisting mass was attached to the moment where the relay switched from the resistor circuit to the solar cell circuit was important. On

the other hand, the energy $E_{\text{solar with}}$ required during the part from the changeover of the relay until the rope on which the assisting mass hangs was completely uncoiled was relevant. Both parts were compared to the energy consumption of the parts before ($E_{\text{resistor without}}$) and after ($E_{\text{solar without}}$) the relay switched in the operation without an assisting mass. The lengths of the compared segments had to be the same. By multiplying the average power over these parts with the time passed, which was taken from the Tracker data, the generated and consumed energies were calculated. The electrical energy $E_{\text{deficit gained}}$ that was lost due to the deceleration by the assisting mass could be determined using the formula below:

$$E_{\text{deficit gained}} = E_{\text{resistor without}} - E_{\text{resistor with}} = 0.01\,\text{J} \tag{29}$$

The energy saved E_{saved} due to the accelerating support by the assisting mass was calculated as follows:

$$E_{\text{saved}} = E_{\text{solar without}} - E_{\text{solar with}} = 0.77\,\text{J} \tag{30}$$

Because there was energy saved in the operation with an assisting mass, the main mass could be pulled up higher than in the operation without an assisting mass with the same amount of electrical energy input. Aided by the round-trip efficiency of the operation with an assisting mass (see Sec. 4.1.1), the ensuing formula determines how much electrical energy flowing over the resistor $E_{\text{potentially gained}}$ corresponds to the saved energy:

$$E_{\text{potentially gained}} = E_{\text{saved}} \cdot \eta_{\text{round-trip}} = 0.05\,\text{J} \tag{31}$$

4.1.5 Energy Consumption of the Electronic Control Unit

To determine the energy consumption of the electronic control unit, first the energy consumption of the single components was calculated. This was done by taking the peak power to the time when the component was used. Then the peak power was subtracted by the average power from before and after the increase of the power value. For the switch of the relay to the consumer[7] circuit, only the power average from before was subtracted, as there was no power measurement

[7] LEDs or a resistor

available afterwards. Then this difference was multiplied with the time of the signal, which was given by the delay in the programming code (see Appendix B). The energy consumption of each component is listed below:

- Servo motor (connect dynamic spool frame): 0.16 J
- Servo motor (disconnect dynamic spool frame): 0.13 J
- Servo motor (connect brake): 0.14 J
- Servo motor (release brake): 0.10 J
- Relay (switch to solar cell circuit): $0.000\,03\,\mathrm{J} \approx 0\,\mathrm{J}$
- Relay (switch to consumer circuit): $0.000\,01\,\mathrm{J} \approx 0\,\mathrm{J}$

Another value needed to calculate the energy consumption was the average power between the utilisation of the components $P_{\text{base load}}$, which amounted to 0.41 W. The energy consumption of an operation that lasted for a time $t_{\text{operation}}$ was determined as outlined below:

$$E = E_{\text{components included}} + P_{\text{base load}} \cdot t_{\text{operation}}\,, \tag{32}$$

where $E_{\text{components included}}$ was the total energy consumption of all components included.

One cycle of the operation without an assisting mass took around 50.8 seconds. During this time the relay switched once in both directions. Therefore, the electronic control unit was in need of 20.9 J. The operation with an assisting mass lasted around 61.3 seconds. It had the same delay times between the code for the acceleration at the top and the deceleration at the bottom. During this operation, the relay switched once forth and back again, and the brake braked and released once. The dynamic spool frame connected and disconnected each two times. Through that an energy consumption of 26.0 J was calculated.

In the final operation, buttons were pressed to change the direction of the main mass by utilising the assisting mass. The pressing of those buttons did not visibly consume energy. When no button was pressed, the power that the electronic control unit took was 0.44 W. For instance, if the main mass moved up for half a minute without interfering, the control unit would consume 13.2 J in this time. When the button was pressed to start the downward motion, the components behaved as follows: the relay switched to the consumer circuit, the dynamic spool frame at-

tached, the brake released, and the dynamic spool frame detached again. This took around 2.3 seconds. Therefore, it was in need of 1.3 J. When the button for the upward motion was pushed, the following actions were carried out by the components: the dynamic spool frame attached, and the relay switched to the solar cell circuit. Later the brake braked, and the dynamic spool frame detached again. This process took around 8.5 seconds. Hence, it consumed 3.9 J. A closer description of this process is outlined in the last paragraph of Section 3.2.

4.2 Projected Values of the SGES Model in Real Size

This subchapter explains how the SGES model would approximately look in reality. It especially highlights how the energy consumption of the electronic control unit and the round-trip efficiency would change.

4.2.1 Application in a Single-Family House

The performance of this model was transferred onto a single-family house with 4 residents, who heat with a heat pump. Based on estimations of the energy consumption of such a household (BFE, 2021) and a sample calculation for an air source heat pump (Hoval, n.d.), an annual energy consumption of 7000 kWh was estimated. By using this value, it was determined that during 6 hours, on average, 17 260 000 J were consumed, which correspond to approximately 5 kWh.

The efficiency $\eta_{\text{small motor}}$ of the motor included in the model was assumed to be 40 %, which was a bit smaller than the maximal efficiency of this motor given in the datasheet (Shenzhen Hua Chuang Sheng Motor Co., 2014, p. 4). An electric motor in reality has usually an efficiency from 70 % to 96 % (Demirel, 2018). For the calculations, an estimated value of 80 % was used as efficiency $\eta_{\text{real motor}}$. When the efficiency $\eta_{\text{small scale, downwards}}$ was taken from the operation with an assisting mass (see Sec. 4.1.1), the efficiency $\eta_{\text{reality, downwards}}$ of the conversion from mechanical potential energy to electrical energy with a real electric motor could be calculated:

$$\eta_{\text{reality, downwards}} = \frac{\eta_{\text{small scale, downwards}}}{\eta_{\text{small motor}}} \cdot \eta_{\text{real motor}} = \frac{0.248}{0.40} \cdot 0.80 \approx 50\,\% \tag{33}$$

Thus, the mechanical potential energy needed would be approximately 35 000 000 J. Additionally, it was assumed that a main mass of 35 000 kg would be taken, which is the same block mass as Energy Vault uses (see Sec. 2.1.1). With these figures and the formula for potential energy in Equation (2), it was determined that an approximate height of 100 m would be necessary to store the energy for a four-person household in a single-family house with a heat pump for six hours.

4.2.2 Energy Consumption of the Electronic Control Unit

In addition to the energy demand of the household, there would be the energy consumption of the SGES system itself. It was estimated how much the electronic control unit would consume over twelve hours, during which the main mass would be accelerated once at the top and decelerated once at the bottom by an assisting mass. That corresponds to one full cycle, assuming that the main mass would also need six hours to be pulled up to the top.

The power $P_{\text{base load}}$ that the Arduino requires if no button is pushed would remain the same. The only difference would be that it would be taken over a longer time period $t_{\text{operation}}$, namely 12 h. Consequently, the energy $E_{\text{base load}}$ that the Arduino would require was calculated like this:

$$E_{\text{base load}} = P_{\text{base load}} \cdot t_{\text{operation}} = 0.44\,\text{W} \cdot 43\,200\,\text{s} \approx 20\,000\,\text{J} \tag{34}$$

The electronic components were treated differently. While it was assumed that the relays require more or less the same energy, the servo motors would have to do more work because the components would be heavier and have to be moved over a greater distance. The aim was to calculate a ratio that describes how much more work would have to be done and, therefore, to determine how much more electrical energy the servos would require. The relevant work was, in this case, the work done against friction (see Eq. (6)). It was ignored that the coefficient μ_k changed, and that it first had to overcome static friction. The gravitational constant is constant. Therefore, the change in mass and distance was primarily important. The formula $m = \rho \cdot V$ (Wetzel, 2019) shows that the mass increases with the volume and the density of an object. Thus, the increases in volume and density, and consequently mass were considered, as well as

the increase in the distance moved.

To simplify the calculation of the increase in volume, the components were seen as cuboid. The dynamic spool frame is 0.09 m long, 0.055 m wide, and 0.06 m high. In real size, the length could be 1.8 m, the width 1.1 m, and the height 1.2 m. The dimensions of the brake are a length of 0.047 m, a width of 0.006 m, and a height of 0.008 m. In reality, it may be 0.94 m long, 0.12 m wide, and 0.16 m high. Thus, the volume was estimated to raise by 8000 from the model to the real size.

The density of steel is 7800 $\frac{\text{kg}}{\text{m}^3}$ (Urone et al., 2022, p. 442), while the density of PLA, the material used in the model, amounts to 1300 $\frac{\text{kg}}{\text{m}^3}$ (extrudr, 2024). It was neglected that the 3D-printed dynamic spool frame had only forty percent infill, whereas the brake had one hundred percent infill. For both, the given density of PLA was used. Therefore, the density was assumed to increase by 6.

As a result, the mass of the brake would increase by 48 000. The distance the brake had to move was estimated to raise from 0.004 m to 0.08 m by 20. The ratio by which the work increases would consequently be 960 000.

To calculate the change in mass of the dynamic spool frame, different elements had to be considered. The changes in mass of the attached servo motor and the rope were assumed to have no major effect, whereas the change in mass of the assisting mass hanging on it could be taken into account. To calculate the mass of the assisting mass, it was assumed that the ratio between the main mass (0.987 kg) and the assisting mass (0.469 kg) would stay the same. Before, it was hypothesised that the main mass would amount to 35 000 kg (see Sec. 4.2.1). Hence, the assisting mass would be about 16 631 kg. The ratio of the mass of the dynamic spool frame itself would be 48 000 as for the brake. As a result, the mass of 0.068 kg of the small-scale dynamic spool frame would amount to 3264 kg in reality. The masses of the dynamic spool frame and the assisting mass were added in small scale and in real size. From these results, it was calculated that its mass would increase by around 37049. The distance, which was initially 0.004 m, was also assumed to grow by 20. Thus, the work would increase by 740 976.

The ratio of the increase in work was multiplied with the measured electrical energy consumption of the respective servo motors. With these new figures in addition to the old ones, the total

energy consumption of the electronic control unit for the acceleration at the top ($E_{\text{acceleration}}$) and the deceleration at the bottom ($E_{\text{deceleration}}$) could be calculated the same way as for the small-scale model in Equation (32). Then they were added together with the result gained in Equation (34):

$$E = E_{\text{acceleration}} + E_{\text{deceleration}} + E_{\text{base load}} \approx 310\,000\,\text{J} + 340\,000\,\text{J} + 20\,000\,\text{J} = 670\,000\,\text{J} \quad (35)$$

Hence, one cycle of the SGES model in a realistic size would require 0.19 kWh of electrical energy.

4.2.3 Round-Trip Efficiency

The round-trip efficiency would also vary if the motor efficiency was adjusted. To calculate this, the round-trip efficiency $\eta_{\text{small scale, round-trip}}$ of the operation with an assisting mass was utilised (see Sec. 4.1.1). In a full cycle, the energy passes two times through the motor. Therefore, the round-trip efficiency $\eta_{\text{reality, round-trip}}$ would look as follows:

$$\eta_{\text{reality, round-trip}} = \frac{\eta_{\text{small scale, round-trip}}}{\eta^2_{\text{small motor}}} \cdot \eta^2_{\text{real motor}} = \frac{0.070}{0.40^2} \cdot 0.80^2 = 28.0\,\% \quad (36)$$

With this efficiency, the energy required to pull up the mass, so that later 17 260 000 J would be released, could be calculated. This energy would amount to approximately 61 620 000 J, which equals 17.12 kWh. When the energy consumption of the electronic control unit was added to the input energy, the efficiency was estimated to be 27.7 %.

5 Discussion

In the discussion, it is shown how the results were calculated and how reliable these results are. Another part is the interpretation of these results, where their meaning is explained. Finally, the SGES technology is compared to alternative technologies.

5.1 Calculation Methods

In the Sections 4.1.1, 4.1.3, and 4.1.4, the energies were calculated by multiplying the elapsed time t with the average power P_{average} during this time period. In this time elapsed, n-power values were measured at intervals of $\frac{t}{n}$. In this approach, for simplicity, it was assumed that the power measured in a time interval $\frac{t}{n}$ remained constant throughout this time interval. Therefore, the energy generated or used could be defined as the sum of all power values multiplied by the time interval. The following calculation shows the connection to the average power:

$$P_1 \cdot \frac{t}{n} + P_2 \cdot \frac{t}{n} + \ldots + P_\text{n} \cdot \frac{t}{n} = \frac{P_1 + P_2 + \ldots + P_\text{n}}{n} \cdot t = P_{\text{average}} \cdot t \tag{37}$$

To select the power values for the average power calculation, the exact time frame defined by the Tracker data was rounded to the less precise time intervals of the current and voltage measurements. Sometimes it was not rounded mathematically. For instance, it would have been necessary to round down, but because the change happened in between, the previous value was not affected by the change. Therefore, the time value was rounded up.

After the energies transferred in the single parts of the measurement were calculated, the efficiency as well as the energy differences due to the assisting mass were determined. In order to do this, it was important to take parts of the measurements where the main mass moved over the same distance. Since the displacement was identical, the mechanical potential energy did not vary, and therefore the two segments were comparable in terms of the electrical energy consumed or released.

Another result was the maximum energy storage capacity of the SGES model (see Sec. 4.1.2). Its calculation required the measurement of the maximum possible height that the main mass

could move upwards. A gap was left between the highest point and the spool because the mass should not hit the armature.

A further result was the energy consumption of the electronic control unit (see Sec. 4.1.5). To calculate the energy demand of the servo motors and the relay, only the peak powers at the time of their utilisation were taken because the measurement devices required time to adapt to the fast-changing voltages and currents. This adaptation took longer than the signal shown in the programming code lasted. Therefore, the time values were taken from the programming code as they seemed more appropriate.

During the analysis of the energy consumption of the electronic control unit, the energy demand during the measurements with and without an assisting mass was also considered. The cycle of the operation without an assisting mass lasted shorter because, for both measurements, the same durations were taken for the upward and the downward motion. However, the use of the assisting mass took additional time, during which the main mass was accelerated and decelerated. The operation without an assisting mass also required some time to accelerate at the top and a brief moment to decelerate and accelerate at the bottom, which happened within the downward and the upward motion. Consequently, the corresponding cycle of the operation with an assisting mass would be slightly shorter. However, this difference had no significant impact and was ignored.

5.2 Accuracy of the Results

The results of these calculations were not that precise due to inaccurate measurement devices. In particular, the measurement of the current and the voltage could not be as accurate because the values were read off from the multimeters in the videos. Nevertheless, Tracker had also some problems. Due to the oscillation of the mass back and forth, it appeared in Figure 25 that the assisting mass was going up and down. Additionally, the velocity of the main mass pointed sometimes into the wrong direction, which could also be due to a slight oscillation. However, the main mass oscillated less because it was not moved by the dynamic spool frame like the assisting mass.

Moreover, the different energy consumption values of the servo motors on the built model were close to each other (see Sec. 4.1.5). It was difficult to say which movement really required more energy. This inaccuracy became even worse when multiplying the values to get figures for the calculations of a realistic size.

5.3 Interpretation of the Results

In this subchapter the outcomes of the measurements are interpreted. It is also demonstrated how the SGES model could be implemented in reality.

5.3.1 Meaning of the Efficiency

The energy losses during the operation reduced the efficiency. They were a result of friction in the mechanical part of the model as well as the losses in the DC motor, which has a relatively low efficiency compared to normal DC motors (see Sec. 4.2.1). To calculate the round-trip efficiency, the energy consumption of the electronic control unit was ignored because its energy consumption was relatively high compared to the maximum storage capacity of the SGES model. The round-trip efficiency of the operation was determined to be 6.2 % without an assisting mass, while it was calculated to be 7.0 % with an assisting mass (see Sec. 4.1.1). This difference could be explained by an inaccuracy of the measurement devices or an occasionally varying behaviour of the model. Both would result in a deviation in the efficiency of each operation.

5.3.2 Usefulness of the Assisting Mass

The usefulness of the assisting mass was one question of this analysis. It was determined with the calculations in Section 4.1.3 and Section 4.1.4. The deceleration at the lowest point by the assisting mass, which was used to support the upward motion again, was proved to be helpful. Through the acceleration help of the assisting mass 0.77 J (see Eq. (30)) of energy from the solar cells were saved. This energy could be used to pull up the main mass even higher, increasing the energy output by 0.05 J (see Eq. (31)). The electrical energy lost due to the deceleration

was only 0.01 J (see Eq. (29)). Hence, this process saved energy.

It was not that evident if the acceleration at the top was beneficial. The first intention that it would be necessary to overcome static friction was proved to be wrong. Nevertheless, it resulted in a slightly faster acceleration time, which meant that the electrical power output was constant sooner. While the acceleration without an assisting mass took around 3.5 s, with an assisting mass the acceleration time amounted only to approximately 1.8 s. However, this process led to a loss of energy. The additional energy needed to raise the assisting mass amounted to 0.91 J (see Eq. (25)). If it had been utilised only to pull up the main mass, it would have led to an additional output of 0.06 J (see Eq. (26)). The use of the assisting mass only resulted in a surplus of 0.02 J electrical energy output (see Eq. (27)). This was likely caused by the additional friction of the connection to the assisting mass.

Furthermore, a disadvantage of the assisting mass was that it required more components of the electronic control unit, for instance, the servo motors. Subsequently, the energy consumption of the electronic control unit is examined in more detail.

5.3.3 Impact of the Electronic Control Unit

The assessment of the electronic control unit, based on the results in Section 4.1.5, showed that the Arduino consumed the most energy due to its base load. The relay and the servo motors were only responsible for a small part of the energy demand. As a result, the utilisation of an assisting mass, and therefore the servo motors, had a small impact.

In the results, it appears that the base load energy demand of the Arduino decreased while pressing the button. Before, the average power had been 0.44 W, while over the whole period after the pressing, it was 0.41 W on average. However, in the first period before something happened and after the button was pressed, the power was higher. It sank during the connection movement of the dynamic spool frame (Table 28). This may have happened because the battery released energy and, therefore, could provide less power afterwards. Regardless of the reason, the difference was small and thus of little relevance.

5.3.4 Real Size Application

After assessing the outcomes of the measurements with the built model, it was noteworthy to know how the model would perform in reality. According to the results (see Sec. 4.2), the model would need a height of about 100 m and a mass of 35 t to store the energy demand of a single-family house with an air source heat pump for six hours. This could be realised by digging a hole to reach this height and not shade potentially existing solar panels. However, for a single-family house, it would be a complex construction that would require much space for a comparably small energy capacity.

Additionally, it is necessary to mention that, to ensure the safety, the model would need more components in reality. For instance, it would require more brakes and a more complex programming of the electronic control unit, such as an emergency stop function. Furthermore, the oscillation of the assisting mass would be a problem in reality, as it would pose a danger. This problem could be solved by inserting an additional gear wheel in between to connect and disconnect the assisting mass with the main mass instead of moving the dynamic spool frame.

Nevertheless, the transfer of the SGES model figures into a realistic size showed that the impact of the energy consumption by the electronic control unit would be lower than in the built model. While, in the constructed model, it would reach already after seven seconds the total releasable energy capacity of the model itself, in the real scale calculations it reduced the efficiency only by 0.3 percentage points. As a result, the impact of the additional components required to use the assisting mass remained small, although the real servo motors had a larger impact on the energy consumption of the electronic control unit (see Sec. 4.2.2).

5.4 Comparative Analysis of Energy Storage Technologies

As seen in the previous section, SGES systems are impractical on the scale of a house. Therefore, they are currently implemented on a larger scale (see Sec. 2.1.1). The evaluation of these systems in comparison to other storage technologies is the subject of this chapter.

5.4.1 Comparison of SGES and PHES

	SGES	PHES
Round-trip efficiency (%)	$75-90$	$65-80$
Energy density ($\frac{\text{kWh}}{\text{m}^3}$)	$2-5$	$0.13-0.5$
Power density ($\frac{\text{kW}}{\text{m}^3}$)	3	$0.01-0.12$
Response time	seconds	minutes
Lifetime (years)	$35-50$ years	$30-60$ years
Self-discharge rate (%)	≈ 0	≈ 0
Levelized cost of electricity ($\frac{\text{Rp.}}{\text{kWh}}$)	$2.2 \sim 2.6$	$3.1 \sim 3.7$

Table 1: Figures of different mechanical energy storage systems (Tong, Lu, Chen, et al., 2022, p. 24), (He et al., 2021, p. 8)

Pumped hydropower energy storage (PHES) is the most mature energy storage technology. On the contrary, there is solid gravity energy storage (SGES) as an emerging large-scale technology. (Tong, Lu, Sun, et al., 2022, pp. 927-928)

The first criteria of comparison are visualised by Table 1. Regarding the round-trip efficiency, the SGES lies on average ten percentage points ahead. However, the best PHES systems are superior to the worst SGES systems. Furthermore, when considering the energy density and the power density, the SGES performs better. Considering the response time, it is visible that the SGES responds within seconds, while the PHES needs some minutes to react. Regarding the lifetime, the PHES has a wider range. That implies that there are more short-lived as well as more durable PHES than SGES. With regard to the self-discharge rate, there is no recognisable difference due to the fact that both technologies have nearly no standing losses. And finally, the compared levelized costs of electricity show that SGES is slightly cheaper.

SGES systems have a versatile energy-to-power ratio. This means that they can provide a high power over a short time or less power over more time. The technology of Gravitricity has a ratio of 15 minutes to 8 hours, while the ratio of Energy Vault's technology is 4 to 24 hours. (Energy Vault, 2024a; Gravitricity, 2024) On the contrary, the typical energy-to-power ratio of PHES is two to eight hours (Blank et al., 2015).

Focusing on the depth discharge limit, the research shows that PHES can be discharged up to $80-100\%$. These values lie in a defined water level range with a minimum and a maximum

point. However, due to the ecosystem, natural lakes have a considerably high minimal water level. (Blank et al., 2015) In contrast to that, SGES has no depth discharge limit (Gravitricity, 2024).

Regarding the adaptability of the energy storage systems, it is visible that SGES adapts well to the topography because it uses dense solid material to store the energy. On the contrary, PHES uses water, which makes it highly dependent on the environment. (Tong, Lu, Chen, et al., 2022, p. 3) Additionally, PHES is exposed to environmental conditions, such as changes in the flow of the stream, deterioration of land structure, sediments in the water, and water evaporation. (Oymak & Tür, 2022, p. 208) Furthermore, the construction of reservoirs and large dams forces local communities to move away, and it affects the natural environment in this region (Blume-Werry & Everts, 2022).

5.4.2 Strengths and Weaknesses of SGES Compared to Other Technologies

In addition to comparing SGES to PHES, it is important to consider its strengths and weaknesses. These were analysed relative to lithium-ion batteries (LIB), redox flow batteries (RFB), and hydrogen energy storage (HES).

	SGES	LIB	RFB	HES
Round-trip efficiency (%)	75 - 90	75 - 90	65 - 85	10 - 40
Energy density ($\frac{kWh}{m^3}$)	2 - 5	100 - 500	16 - 30	500 - 3000
Self-discharge rate (%)	≈ 0	5 per month	0.1 - 0.4 per day	≈ 0

Table 2: Figures of various energy storage systems (Tong, Lu, Chen, et al., 2022, p. 24), (He et al., 2021, p. 8), (Elalfy et al., 2024, p. 12), (IEC, 2020)

A key strength of SGES is that it has no self-discharge (Table 2). Whereas the self-discharge rate of LIB is 5 % per month, and for the RFB it is 0.1 to 0.4 % per day. Only the HES can keep up with the SGES.

However, in terms of efficiency, HES is far behind SGES at 10 to 40 % (Table 2). The efficiencies of LIB and SGES are similar, while the redox flow batteries are only slightly behind.

On the contrary, a major weakness of SGES is the small energy density. With 2 to 5 $\frac{kWh}{m^3}$ (Table

2), SGES lies behind the RFB. The LIB and HES surpass it even further.

An additional strength is that SGES does not deteriorate, and unlike in electrochemical batteries, the storage capacity remains constant over time (Jorio & Zhang, 2024). In the case of HES, the components of the fuel cells and electrolysers are affected by degradation due to electrical, mechanical, and thermal deformation. That results in a performance loss. (Yue et al., 2021, p. 22)

Another advantage of SGES is its sustainability. This means it does not produce pollution, has no risk of fire or explosion, and is therefore safe. (Tong, Lu, Chen, et al., 2022, p. 25) In contrast, lithium-ion batteries are associated with fire risk, which decreases their safety (Shoushtari & Li, 2023, p. 78). Although lithium is not a rare raw material, the mining thereof is environmentally unfriendly because it requires much water, and the chemicals used for the extraction contaminate the water. Even though lithium exists in Europe, it comes mainly from Chile, Australia, and Argentina. (Widmann et al., 2022) Also, the redox flow batteries are associated with environmental issues (Elalfy et al., 2024, p. 12). With regard to HES, rare materials are used as catalysts of electrodes, electrolyte additives, and for other purposes. Additionally, hydrogen itself may be considered an indirect greenhouse gas. During production, transport, and use, 0.2 to 10 percent of the hydrogen is emitted. (Yue et al., 2021, p. 21)

Despite the advantages over batteries, SGES faces a drawback in terms of the response time. For SGES, it is in the range of seconds, while batteries respond within ten milliseconds. (Tong, Lu, Chen, et al., 2022, p. 24)

Another weakness compared to batteries is that SGES proves uneconomical in small-scale scenarios (Tong, Lu, Chen, et al., 2022, p. 25). On the contrary, batteries for small residential PV systems are already profitable (Hoppmann et al., 2014, p. 28).

6 Conclusion

In summary, it can be said that the most important components to store energy by utilising a mass are a spool to wind up the rope attached to the mass and a motor to convert between the electrical and the mechanical energy. Additionally, a gear unit is required, such that the rotational frequency at the motor is high, but the mass moves slowly. Buttons can be utilised to control the solid gravity energy storage system, while the use of the relay is to switch between the producer and the consumer circuit. In addition, the dynamic spool frame, which holds the assisting mass, can be attached by a servo motor. Another servo motor can be used to brake the gear wheel of the assisting mass.

It was found that the assisting mass can be used for two main purposes. Firstly, it saves energy by decelerating and accelerating the main mass at the lowest point. Secondly, it makes it possible to achieve a constant power output sooner with the acceleration at the top, but this results in a loss of energy.

In addition to these findings, the key performance indicators of the SGES model were determined. It has an efficiency of $6-7\,\%$ and a maximum possible energy output of $2.88\,\mathrm{J}$ after it has been fully charged. If the assisting mass needs to accelerate the main mass at the top, the electronic control unit requires $1.3\,\mathrm{J}$. Furthermore, it requires $3.9\,\mathrm{J}$ during the period when the assisting mass decelerates the main mass, supports its upward acceleration, and then is pulled up itself. In between, a power of $0.44\,\mathrm{W}$ is required.

The SGES model has some weaknesses that could be improved. For instance, the gear wheels sway forth and back a little, which can cause them to block each other. In addition, there are only two options to control the model with the electronic control unit. Different functions could be added, such as a complete stop of the motion for a longer time, sensors that recognise if the main mass is at the top, and brakes that directly connect to the main gear unit.

Despite these issues, a strength of the model is that it can be controlled by simply pushing buttons. Another quality lies in the fact that the energy during the braking process is not completely lost due to the assisting mass. A further benefit of the assisting mass is the sooner establishment of a constant power output.

Additionally, the findings of the model were transmitted on a household with four people living in a single-family house with an air source heat pump. This household was assumed to have an energy demand of 5 kWh in six hours. To store this amount of energy, a mass of 35 t, which can be pulled up about 100 m, would be necessary. The electronic control unit would require 0.19 kWh for one cycle, which was estimated to last twelve hours. This would not heavily affect the round-trip efficiency, unlike in the small-scale model. The efficiency adapted to a real DC motor would be about 28 %. The dimensions required to store 5 kWh show that SGES is too complex for an application on the scale of a single-family house.

Therefore, SGES is mainly utilised in larger units. This technology was compared to conventional energy storage systems. The principle of pumped hydropower energy storage is similar to SGES. Even though PHES is more mature, SGES has some advantages over PHES. For instance, it performs better regarding the round-trip efficiency, the energy density, the response time, and the levelized cost of electricity. Additionally, SGES adapts better to its environment than PHES. In comparison to lithium-ion batteries, redox flow batteries, and hydrogen energy storage, SGES is in arrears regarding the energy density, the response time, and the profitability in small-scale scenarios. However, its upsides are the high efficiency, the sustainability, and the absence of self-discharge as well as deterioration.

Overall, the constructed model makes it possible to demonstrate and understand how SGES systems work. The comparison to alternative energy storage systems reveals that SGES is an uprising energy storage system, which can reduce the problem of the lack of storage facilities.

To further examine the model, more accurate measurement devices should be used. This would lead to more meaningful results, which would result in further findings about the exact behaviour of the model.

Further studies could be carried out to monitor the future development of solid gravity energy storage. In particular, the outcomes of the different projects outlined in Section 2.1.1 are expected to provide valuable insights. Additionally, SGES could be compared to further energy storage technologies.

Appendix A: Data Tables for the Calculations

Calculation of the Efficiency of the Operation Without an Assisting Mass

Time (s)	Position (m)
17.935	0.774
25.570	0.874

Table 3: Upward motion (position data)

Time (s)	Voltage (V)	Current (A)	Power (W)
18	3.21	0.1465	0.470265
19	3.21	0.1465	0.470265
20	3.32	0.1436	0.476752
21	3.37	0.1438	0.484606
22	3.19	0.1466	0.467654
23	3.33	0.1457	0.485181
24	3.38	0.1423	0.480974
25	3.19	0.1466	0.467654
26	3.29	0.1457	0.479353

Table 4: Upward motion (power data)

Time (s)	Position (m)
40.005	0.757
43.972	0.657

Table 5: Downward motion (position data)

Time (s)	Voltage (V)	Current (A)	Power (W)
40	2.37	0.0233	0.055221
41	2.42	0.0239	0.057838
42	2.36	0.0235	0.05546
43	2.42	0.024	0.05808
44	2.38	0.0239	0.056882

Table 6: Downward motion (power data)

Calculation of the Efficiency of the Operation With an Assisting Mass

Time (s)	Position (m)
10.002	0.584
16.602	0.684

Table 7: Upward motion (position data)

Time (s)	Voltage (V)	Current (A)	Power (W)
10	3.45	0.1497	0.516465
11	3.47	0.148	0.51356
12	3.6	0.1473	0.53028
13	3.43	0.149	0.51107
14	3.5	0.148	0.518
15	3.58	0.1461	0.523038
16	3.42	0.1506	0.515052
17	3.46	0.1499	0.518654

Table 8: Upward motion (power data)

Time (s)	Position (m)
42.005	0.867
46.105	0.767

Table 9: Downward motion (position data)

Time (s)	Voltage (V)	Current (A)	Power (W)
42	2.43	0.0241	0.058563
43	2.43	0.0241	0.058563
44	2.43	0.0241	0.058563
45	2.44	0.0241	0.058804
46	2.4	0.024	0.0576

Table 10: Downward motion (power data)

Calculation of the Acceleration at the Top

Time (s)	Position (m)
2.167	0.512
6.335	0.540

Table 11: Upward motion (with assisting mass, position data)

Time (s)	Voltage (V)	Current (A)	Power (W)
2	4.67	0.1175	0.548725
3	3.6	0.1384	0.49824
4	2.54	0.1638	0.416052
5	2.31	0.1663	0.384153
6	2.32	0.1664	0.386048

Table 12: Upward motion (with assisting mass, power data)

Time (s)	Position (m)
4.000	0.582
5.968	0.610

Table 13: Upward motion (without assisting mass, position data)

Time (s)	Voltage (V)	Current (A)	Power (W)
4	3.39	0.1435	0.486465
5	3.33	0.1459	0.485847
6	3.21	0.1487	0.477327

Table 14: Upward motion (without assisting mass, power data)

Time (s)	Position (m)
37.138	0.970
41.472	0.881

Table 15: Downward motion (with assisting mass, position data)

Time (s)	Voltage (V)	Current (A)	Power (W)
37.2	0.22	0.0038	0.000836
37.4	0.22	0.0032	0.000704
37.6	0.04	0.0038	0.000152
37.8	0.689	0.003	0.002067
38.0	0.689	0.003	0.002067
38.2	1.38	0.0178	0.024564
38.4	1.38	0.0178	0.024564
38.6	1.897	0.0223	0.0423031
38.8	1.897	0.0223	0.0423031
39.0	2.49	0.0249	0.062001
39.2	2.49	0.0249	0.062001
39.4	2.49	0.0249	0.062001
39.6	2.5	0.0249	0.06225
39.8	2.5	0.0249	0.06225
40.0	2.5	0.0245	0.06125
40.2	2.43	0.0245	0.059535
40.4	2.43	0.0241	0.058563
40.6	2.44	0.0244	0.059536
40.8	2.44	0.0244	0.059536
41.0	2.44	0.0242	0.059048
41.2	2.44	0.0242	0.059048
41.4	2.44	0.0241	0.058804

Table 16: Downward motion (with assisting mass, power data)

Time (s)	Position (m)
31.703	0.947
36.037	0.858

Table 17: Downward motion (without assisting mass, position data)

Time (s)	Voltage (V)	Current (A)	Power (W)
32.0	0.432	0.0043	0.0018576
32.5	1.319	0.0142	0.0187298
33.0	1.615	0.0169	0.0272935
33.5	1.983	0.0157	0.0311331
34.0	2.17	0.0214	0.046438
34.5	2.21	0.0222	0.049062
35.0	2.33	0.0222	0.051726
35.5	2.38	0.0234	0.055692
36.0	2.37	0.0235	0.055695

Table 18: Downward motion (without assisting mass, power data)

Calculation of the Deceleration at the Bottom

Time (s)	Position (m)
62.973	0.391
64.007	0.423

Table 19: Upward motion (with assisting mass, position data)

Time (s)	Voltage (V)	Current (A)	Power (W)
63.0	3.62	0.1581	0.572322
63.2	3.62	0.1581	0.572322
63.4	4.15	0.1412	0.58598
63.6	4.15	0.1833	0.760695
63.8	4.61	0.1137	0.524157
64.0	4.61	0.1137	0.524157

Table 20: Upward motion (with assisting mass, power data)

Time (s)	Position (m)
51.572	0.458
54.840	0.489

Table 21: Upward motion (without assisting mass, position data)

Time (s)	Voltage (V)	Current (A)	Power (W)
51.6	1.97	0.1508	0.297076
51.8	1.898	0.1508	0.2862184
52.0	1.898	0.1544	0.2930512
52.2	1.898	0.1544	0.2930512
52.4	2.72	0.1577	0.428944
52.6	2.72	0.1577	0.428944
52.8	2.93	0.1518	0.444774
53.0	2.93	0.1518	0.444774
53.2	3.11	0.1463	0.454993
53.4	3.23	0.1443	0.466089
53.6	3.23	0.1443	0.466089
53.8	3.28	0.1439	0.471992
54.0	3.28	0.1439	0.471992
54.2	3.34	0.1433	0.478622
54.4	3.35	0.1428	0.47838
54.6	3.35	0.1426	0.47771
54.8	3.35	0.141	0.47235

Table 22: Upward motion (without assisting mass, power data)

Time (s)	Position (m)
59.673	0.416
62.973	0.391

Table 23: Downward motion (with assisting mass, position data)

Time (s)	Voltage (V)	Current (A)	Power (W)
59.8	2.5	0.024	0.06
60.0	2.5	0.024	0.06
60.2	2.25	0.0183	0.041175
60.4	2.25	0.0183	0.041175
60.6	1.275	0.0126	0.016065
60.8	1.275	0.0126	0.016065
61.0	1.005	0.0088	0.008844
61.2	1.005	0.0088	0.008844
61.4	0.685	0.0057	0.0039045
61.6	0.685	0.0057	0.0039045
61.8	0.446	0.0035	0.001561
62.0	0.251	0.0039	0.0009789
62.2	0.032	0.0011	0.0000352
62.4	0.032	0	0
62.6	0	0	0
62.8	0	0	0

Table 24: Downward motion (with assisting mass, power data)

Time (s)	Position (m)
50.538	0.482
51.572	0.458

Table 25: Downward motion (without assisting mass, position data)

Time (s)	Voltage (V)	Current (A)	Power (W)
50.6	2.48	0.0247	0.061256
50.8	2.49	0.024	0.05976
51.0	2.49	0.0248	0.061752
51.2	2.49	0.0248	0.061752
51.4	1.97	0.0249	0.049053

Table 26: Downward motion (without assisting mass, power data)

Calculation of the Energy Consumption of the Electronic Control Unit

Time (s)	Voltage (V)	Current (A)	Power (W)
1	7.94	0.0555	0.44067
2	7.94	0.0555	0.44067
3	7.93	0.0555	0.440115
4	7.93	0.0555	0.440115

Table 27: Idle electronic control unit (no buttons were pressed)

Time (s)	Voltage (V)	Current (A)	Power (W)
7	7.92	0.0568	0.449856
8	7.92	0.0562	0.445104
9	7.92	0.0562	0.445104
10	7.92	0.0562	0.445104
14	7.95	0.0499	0.396705
15	7.95	0.0498	0.39591
16	7.95	0.0498	0.39591
20	7.94	0.0506	0.401764
21	7.94	0.0507	0.402558
22	7.94	0.0507	0.402558
25	7.93	0.0507	0.402051
26	7.94	0.0508	0.403352
27	7.94	0.0508	0.403352
31	7.93	0.0508	0.402844
32	7.93	0.0508	0.402844
33	7.93	0.0508	0.402844
35	7.93	0.0509	0.403637
36	7.93	0.0508	0.402844
37	7.93	0.0509	0.403637
38	7.92	0.0509	0.403128

Table 28: Idle electronic control unit (after a button has been pressed)

Time (s)	Voltage (V)	Current (A)	Power (W)
11.8	7.78	0.0953	0.741434
12.0	7.78	0.0953	0.741434
12.2	7.88	0.0869	0.684772
12.4	7.88	0.0869	0.684772
12.6	7.94	0.0607	0.481958
12.8	7.94	0.053	0.42082

Table 29: The dynamic spool frame attaches

Time (s)	Voltage (V)	Current (A)	Power (W)
28.0	7.8	0.0531	0.41418
28.2	7.8	0.0831	0.64818
28.4	7.84	0.0839	0.657776
28.6	7.88	0.0772	0.608336
28.8	7.88	0.0772	0.608336
29.0	7.93	0.0585	0.463905
29.2	7.93	0.0585	0.463905
29.4	7.93	0.053	0.42029
29.6	7.93	0.053	0.42029
29.8	7.93	0.0514	0.407602
30.0	7.93	0.051	0.40443

Table 30: The dynamic spool frame detaches

Time (s)	Voltage (V)	Current (A)	Power (W)
17.2	7.75	0.0857	0.664175
17.4	7.86	0.0857	0.673602
17.6	7.86	0.079	0.62094
17.8	7.93	0.079	0.62647
18.0	7.93	0.0605	0.479765
18.2	7.93	0.0535	0.424255
18.4	7.93	0.0535	0.424255
18.6	7.93	0.0515	0.408395
18.8	7.94	0.0515	0.40891

Table 31: The brake connects

Time (s)	Voltage (V)	Current (A)	Power (W)
22.6	7.86	0.0766	0.602076
22.8	7.86	0.0766	0.602076
23.0	7.91	0.0734	0.580594
23.2	7.91	0.0591	0.467481
23.4	7.91	0.0597	0.472227
23.6	7.91	0.0534	0.422394
23.8	7.92	0.0534	0.422928
24.0	7.92	0.0515	0.40788
24.2	7.92	0.0515	0.40788
24.4	7.92	0.051	0.40392

Table 32: The brake releases

Time (s)	Voltage (V)	Current (A)	Power (W)
33.6	7.93	0.0512	0.406016
33.8	7.93	0.0512	0.406016
34.0	7.93	0.051	0.40443
34.2	7.93	0.051	0.40443

Table 33: The relay switches to the electric circuit with the solar cells

Time (s)	Voltage (V)	Current (A)	Power (W)
38.6	7.92	0.051	0.40392
38.8	7.92	0.051	0.40392

Table 34: The relay switches to the electric circuit with the LEDs

Appendix B: Programming Code

Measurement Without an Assisting Mass

```
#include "Servo.h"

Servo servo_w;
Servo servo_b;
int relayset = 5;
int relayreset = 6;
int TasterUp = 9;
int StatusUp = 0;

void setup() {
  pinMode(relayset, OUTPUT);
  pinMode(relayreset, OUTPUT);
  pinMode(TasterUp, INPUT);
}

void relay_solar(){
  digitalWrite(relayset,HIGH);
  delay(10);
  digitalWrite(relayset,LOW);
} #relay switches to the circuit with the solar cells

void relay_led(){
  digitalWrite(relayreset,HIGH);
  delay(10);
  digitalWrite(relayreset,LOW);
} #relay switches to the circuit with the LEDs or the resistor

void loop() {
```

```
29    StatusUp = digitalRead(TasterUp);
30    if (StatusUp == HIGH){
31      delay(10000);
32      relay_solar();
33      delay(50000);
34      relay_led();
35      delay(20000);
36      relay_solar();
37      delay(30000);
38      relay_led();
39    }
40  }
```

Measurement With an Assisting Mass

```
1  #include "Servo.h"
2
3  Servo servo_w;
4  Servo servo_b;
5  int relayset = 5;
6  int relayreset = 6;
7  int TasterUp = 9;
8  int StatusUp = 0;
9  int TasterDown = 10;
10 int StatusDown = 0;
11
12 void setup() {
13   pinMode(relayset, OUTPUT);
14   pinMode(relayreset, OUTPUT);
15   pinMode(TasterUp, INPUT);
16   pinMode(TasterDown, INPUT);
```

```
17 }
18
19 void servowheel_back() {
20   servo_w.attach(8);
21   servo_w.write(75);
22   delay(500);
23   servo_w.detach();
24 } #dynamic spool frame detaches
25
26 void servowheel_forward() {
27   servo_w.attach(8);
28   servo_w.write(40);
29   delay(500);
30   servo_w.detach();
31 } #dynamic spool frame attaches
32
33 void servobrake_brake() {
34   servo_b.attach(7);
35   servo_b.write(10);
36   delay(500);
37   servo_b.detach();
38 } #brake connects
39
40 void servobrake_release() {
41   servo_b.attach(7);
42   servo_b.write(65);
43   delay(500);
44   servo_b.detach();
45 } #brake releases
46
47 void relay_solar() {
48   digitalWrite(relayset, HIGH);
```

```
49    delay(10);
50    digitalWrite(relayset, LOW);
51  } #relay switches to the circuit with the solar cells
52
53  void relay_led() {
54    digitalWrite(relayreset, HIGH);
55    delay(10);
56    digitalWrite(relayreset, LOW);
57  } #relay switches to the circuit with the LEDs or the resistor
58
59  void start() {
60    relay_led();
61    servowheel_forward();
62    delay(100);
63    servobrake_release();
64    delay(1200);
65    servowheel_back();
66  } #acceleration at the top
67
68  void stop() {
69    servowheel_forward();
70    delay(2500);
71    relay_solar();
72    delay(5000);
73    servobrake_brake();
74    servowheel_back();
75  } #deceleration at the bottom, re-acceleration, and pulling up the
       assisting mass
76
77  void loop() {
78    StatusUp = digitalRead(TasterUp);
79    if (StatusUp == HIGH) {
```

```
80      delay(10000);
81      relay_solar();
82      delay(1000);
83      servowheel_forward();
84      delay(4000);
85      servobrake_brake();
86      servowheel_back();
87      delay(50000);
88      start();
89      delay(20000);
90      stop();
91      delay(30000);
92      start();
93      delay(20000);
94      stop();
95      delay(5000);
96      start();
97    }
98  }
```

Measurement of the Electronic Control Unit

```
1  #include "Servo.h"
2
3  Servo servo_w;
4  Servo servo_b;
5  int relayset = 5;
6  int relayreset = 6;
7  int TasterUp = 9;
8  int StatusUp = 0;
9  int TasterDown = 10;
```

```
10 int StatusDown = 0;
11
12 void setup() {
13   pinMode(relayset, OUTPUT);
14   pinMode(relayreset, OUTPUT);
15   pinMode(TasterUp, INPUT);
16   pinMode(TasterDown, INPUT);
17 }
18
19 void servowheel_back() {
20   servo_w.attach(8);
21   servo_w.write(75);
22   delay(500);
23   servo_w.detach();
24 } #dynamic spool frame detaches
25
26 void servowheel_forward() {
27   servo_w.attach(8);
28   servo_w.write(40);
29   delay(500);
30   servo_w.detach();
31 } #dynamic spool frame attaches
32
33 void servobrake_brake() {
34   servo_b.attach(7);
35   servo_b.write(10);
36   delay(500);
37   servo_b.detach();
38 } #brake connects
39
40 void servobrake_release() {
41   servo_b.attach(7);
```

```
42    servo_b.write(65);
43    delay(500);
44    servo_b.detach();
45  } #brake releases
46
47  void relay_solar() {
48    digitalWrite(relayset, HIGH);
49    delay(10);
50    digitalWrite(relayset, LOW);
51  } #relay switches to the circuit with the solar cells
52
53  void relay_led() {
54    digitalWrite(relayreset, HIGH);
55    delay(10);
56    digitalWrite(relayreset, LOW);
57  } #relay switches to the circuit with the LEDs or the resistor
58
59  void loop() {
60    StatusUp = digitalRead(TasterUp);
61    if (StatusUp == HIGH) {
62      delay(5000);
63      servowheel_forward();
64      delay(5000);
65      servobrake_brake();
66      delay(5000);
67      servobrake_release();
68      delay(5000);
69      servowheel_back();
70      delay(5000);
71      relay_solar();
72      delay(5000);
73      relay_led();
```

```
74    }
75  }
```

Final Programming Code

```
1  #include "Servo.h"
2
3  Servo servo_w;
4  Servo servo_b;
5  int relayset = 5;
6  int relayreset = 6;
7  int TasterUp = 9;
8  int StatusUp = 0;
9  int TasterDown = 10;
10 int StatusDown = 0;
11
12 void setup() {
13   pinMode(relayset, OUTPUT);
14   pinMode(relayreset, OUTPUT);
15   pinMode(TasterUp, INPUT);
16   pinMode(TasterDown, INPUT);
17 }
18
19 void servowheel_back(){
20   servo_w.attach(8);
21   servo_w.write(50);
22   delay(300);
23   servo_w.detach();
24 } #dynamic spool frame detaches
25
26 void servowheel_forward(){
```

```
27    servo_w.attach(8);
28    servo_w.write(0);
29    delay(300);
30    servo_w.detach();
31  } #dynamic spool frame attaches
32
33  void servobrake_brake(){
34    servo_b.attach(7);
35    servo_b.write(0);
36    delay(300);
37    servo_b.detach();
38  } #brake connects
39
40  void servobrake_release(){
41    servo_b.attach(7);
42    servo_b.write(55);
43    delay(300);
44    servo_b.detach();
45  } #brake releases
46
47  void relay_solar(){
48    digitalWrite(relayset,HIGH);
49    delay(10);
50    digitalWrite(relayset,LOW);
51  } #relay switches to the circuit with the solar cells
52
53  void relay_led(){
54    digitalWrite(relayreset,HIGH);
55    delay(10);
56    digitalWrite(relayreset,LOW);
57  } #relay switches to the circuit with the LEDs or the resistor
58
```

```
59 void loop() {
60   StatusUp = digitalRead(TasterUp);
61   if (StatusUp == HIGH){
62     servowheel_forward();
63     delay(2500);
64     relay_solar();
65     delay(3500);
66     servobrake_brake();
67     servowheel_back();
68   }
69   StatusDown = digitalRead(TasterDown);
70   if (StatusDown == HIGH){
71     relay_led();
72     servowheel_forward();
73     delay(100);
74     servobrake_release();
75     delay(800);
76     servowheel_back();
77   }
78 }
```

References

Arangarajan, V., M.T.O., A., Chandran, J., Shafiullah, G., & Stojcevski, A. (2015, January). *Role of energy storage in the power system network.* Retrieved 14 October 2024, from https://www.researchgate.net/publication/292682073_Role_of_energy_storage_in_the_power_system_network

Autodesk. (2024). *Tinkercad.* Retrieved 18 October 2024, from https://www.tinkercad.com/

BFE. (2021, August). *Stromverbrauch eines typischen Haushalts.* Retrieved 30 November 2024, from https://pubdb.bfe.admin.ch/de/publication/download/10559

Blanc, C. (2009, April 24). *Modeling of a vanadium redox flow battery electricity storage system.* Retrieved 12 December 2024, from https://infoscience.epfl.ch/entities/publication/23e4c066-99f0-47a3-89e9-ae4d4425faf8

Blank, T., Fuchs, G., Gitis, A., Leuthold, M., Lunz, B., Magnor, D., ... Sauer, D. U. (2015). Pumped Hydro-Energy Storage System. In P. T. Moseley & J. Garche (Eds.), *Electrochemical Energy Storage for Renewable Sources and Grid Balancing* (chap. 7.3.1). München: Elsevier. Retrieved 16 September 2024, from https://www.sciencedirect.com/topics/engineering/pumped-hydro-energy-storage-system

Blume-Werry, E., & Everts, M. (2022, May 28). Hydropower. In M. Hafner & G. Luciani (Eds.), *The Palgrave Handbook of International Energy Economics* (p. 145-156). Cham: Springer International Publishing. Retrieved 6 October 2024, from https://doi.org/10.1007/978-3-030-86884-0_8 doi: 10.1007/978-3-030-86884-0_8

Bundesamt für Statistik. (2023, July 25). *Energieeinfuhr und -ausfuhr.* Retrieved 13 May 2024, from https://www.bfs.admin.ch/bfs/de/home/statistiken/energie.assetdetail.27005042.html

Conrad Electronic. (n.d.-a). *Mini Solar Cell Panel.* Retrieved 30 August 2024, from https://asset.conrad.com/media10/add/160267/c1/-/en/002481807DS00/

datenblatt-2481807-tru-components-poly-pvz-6060-5v-solarzelle-6-vdc-0065-a-1-st-l-x-b-x-h-60-x-60-x-31-mm.pdf

Conrad Electronic. (n.d.-b). *Omron G6AK-274P-ST-US 5 VDC Printrelais 5 V/DC 2 A 2 Wechsler 1 St.* Retrieved 30 August 2024, from https://www.conrad.ch/de/p/omron-g6ak-274p-st-us-5-vdc-printrelais-5-v-dc-2-a-2-wechsler-1-st-503686.html#productDescription

Conrad Electronic. (n.d.-c). *Sol Expert 90002L SOL300 Solarmotor.* Retrieved 30 August 2024, from https://www.conrad.ch/de/p/sol-expert-90002l-sol300-solarmotor-1371438.html

Cuthrell, S. (2024, February 24). *Gravity System Aids Storage in Unused Mine Shaft.* Retrieved 10 July 2024, from https://eepower.com/news/gravity-system-aids-energy-storage-in-unused-mine-shaft/#

Demirel, Y. (2018). Energy Management. In *Motor Efficiency.* Retrieved 2 December 2024, from https://www.sciencedirect.com/topics/engineering/motor-efficiency

Elalfy, D. A., Gouda, E., Kotb, M. F., Bureš, V., & Sedhom, B. E. (2024, July). Comprehensive review of energy storage systems technologies, objectives, challenges, and future trends. *Energy Strategy Reviews*, *54*, 101482. Retrieved 6 October 2024, from https://www.sciencedirect.com/science/article/pii/S2211467X24001895 doi: https://doi.org/10.1016/j.esr.2024.101482

Energy Vault. (2024a). *G-VAULT™.* Retrieved 16 September 2024, from https://www.energyvault.com/products/g-vault

Energy Vault. (2024b). *Rudong, China Gravity Energy Storage System.* Retrieved 7 July 2024, from https://www.energyvault.com/projects/cn-rudong

Energy Vault. (2024c). *Zhangye, China Gravity Energy Storage System.* Retrieved 7 July 2024, from https://www.energyvault.com/projects/zhangye

ESTV. (n.d.). *Monatsmittelkurs (gültig für Juli 2022).* Retrieved 22 December 2024, from https://www.estv.admin.ch/estv/de/home/mehrwertsteuer/mwst-abrechnen/

mwst-fremdwaehrungskurse/archiv-der-monatsmittelkurse/archiv-2022/juli-2022.html

European Association for Storage of Energy. (2024a). *Technologies.* Retrieved 16 May 2024, from https://ease-storage.eu/energy-storage/technologies/

European Association for Storage of Energy. (2024b). *Why Energy Storage?* Retrieved 16 May 2024, from https://ease-storage.eu/energy-storage/why-energy-storage/

extrudr. (2024, June 20). *Technical Data Sheet PLA NX2 MATT.* Retrieved 1 December 2024, from https://s3-extrudr.mgh3.mynet.at/extrudr-media/datasheets/tds/tds-en/pla-nx2-matt-TDS-en.pdf

Faulhaber, F. (n.d.). *Motor Calculations for Coreless Brush DC Motors.* Retrieved 18 July 2024, from https://www.faulhaber.com/en/know-how/tutorials/dc-motor-tutorial-motor-calculations-for-coreless-brush-dc-motors/

Gomstyn, A., & Jonker, A. (2024). *What is energy storage?* Retrieved 24 June 2024, from https://www.ibm.com/think/topics/energy-storage

Gravitricity. (2024). *Technology.* Retrieved 16 September 2024, from https://gravitricity.com/technology/#gravistore

Gravity Power. (n.d.). *Home - Gravity Power.* Retrieved 11 July 2024, from https://www.gravitypower.net/

Gravity Storage. (2024). *Technical Concept.* Retrieved 11 July 2024, from https://gravity-storage.com/technical-concept/

He, W., King, M., Luo, X., Dooner, M., Li, D., & Wang, J. (2021, November 19). Technologies and economics of electric energy storages in power systems: Review and perspective. *Advances in Applied Energy*, *4*, 100060. Retrieved 15 September 2024, from https://www.sciencedirect.com/science/article/pii/S2666792421000524 doi: https://doi.org/10.1016/j.adapen.2021.100060

Hoppmann, J., Volland, J., Schmidt, T. S., & Hoffmann, V. H. (2014, November). The economic viability of battery storage for residential solar photovoltaic systems – A review and a simulation model. *Renewable and Sustainable Energy Reviews*, *39*, 1101–1118. Retrieved 10 October 2024, from https://www.sciencedirect.com/science/article/pii/S1364032114005206 doi: https://doi.org/10.1016/j.rser.2014.07.068

Hoval. (n.d.). *Stromverbrauch von Wärmepumpen: Was Sie wissen sollten.* Retrieved 30 November 2024, from https://www.hoval.ch/de_CH/Stromverbrauch-von-W%C3%A4rmepumpen-%E2%80%93-Effizienz-und-Kosten-%7C-Hoval/wie-viel-strom-benoetigt-eine-waermepumpe

Höfler, A. (2018, August 2). *How does a gearbox (transmission) work?* Retrieved 21 September 2024, from https://www.tec-science.com/mechanical-power-transmission/basics/operating-principle/

IEC. (2020, February 26). *Key new standard for hydrogen storage.* Retrieved 8 October 2024, from https://www.iec.ch/blog/key-new-standard-hydrogen-storage

Jorio, L., & Zhang, Y. (2024, April 25). *Swiss gravity battery contributes to China's energy transition.* Retrieved 10 October 2024, from https://www.swissinfo.ch/eng/science/a-swiss-battery-for-chinas-energy-transition/76328464

Kafader, U. (2019). *maxon Motors as Generators.* Retrieved 20 July 2024, from https://support.maxongroup.com/hc/en-us/articles/360004496254-maxon-Motors-as-Generators

Moore, S. K. (2021, January 5). *Gravity Energy Storage Will Show its Potential in 2021.* Retrieved 16 May 2024, from https://spectrum.ieee.org/gravity-energy-storage-will-show-its-potential-in-2021

Neil. (2023, February 20). *Spur Gear - Custom feature.* Retrieved 22 December 2024, from https://cad.onshape.com/documents/5742c8cde4b06c68b362d748/v/1db29081376c095cf10e2a3d/e/01a666571e625f8b819fd75b

Omron. (n.d.). *PCB Relay.* Retrieved 30 August 2024, from https://asset.conrad.com/media10/add/160267/c1/-/en/000503686DS01/datenblatt-503686-omron-g6ak-274p-st-us-5-vdc-printrelais-5-vdc-2-a-2-wechsler-1-st.pdf

Oymak, A., & Tür, M. R. (2022). An Evaluation of Pumped Hydroelectric Storage Systems. *International Journal of Innovative Engineering Applications*, *6*(2), 205—214. doi: 10.46460/ijiea.1074300

Power HD. (n.d.). *Analog Servo Model No. 1800A.* Retrieved 24 December 2024, from https://www.chd.hk/UploadFiles/Att/2024111314495956.pdf

Sauer, D. U., Fuchs, G., Lunz, B., & Leuthold, M. (2012, June). *Technology Overview on Electricity Storage - Overview on the potential and on the deployment perspectives of electricity storage technologies.* Retrieved 14 October 2024, from https://www.researchgate.net/publication/299425278_Technology_Overview_on_Electricity_Storage_-_Overview_on_the_potential_and_on_the_deployment_perspectives_of_electricity_storage_technologies doi: 10.13140/RG.2.1.5191.5925

Schoenfisch, M., & Dasgupta, A. (2023, July 11). *Grid-scale Storage.* Retrieved 11 July 2024, from https://www.iea.org/energy-system/electricity/grid-scale-storage

Shenzhen Hua Chuang Sheng Motor Co. (2014, September 17). *Product Specification.* Retrieved 30 August 2024, from https://asset.conrad.com/media10/add/160267/c1/-/en/001371438DS01/datenblatt-1371438-sol-expert-90002l-sol300-solarmotor.pdf

Shoushtari, F., & Li, C. (2023, December 23). Feasibility Study for Lithium Ion Battery Production in Uncertainty Situation. *International journal of industrial engineering and operational research*, *5*(5), pp. 76–89. Retrieved 9 October 2024, from https://bgsiran.ir/journal/ojs-3.1.1-4/index.php/IJIEOR/article/view/75

The Pennsylvania State University. (2023). *Overall Efficiency.* Retrieved 2 December 2024, from https://www.e-education.psu.edu/egee102/node/1944#:~:

text=Calculating%20Overall%20Efficiency&text=It%20can%20be%20seen%20that,the%20individual%20subsystems%20or%20processes.

Tong, W., Lu, Z., Chen, W., Han, M., Zhao, G., Wang, X., & Deng, Z. (2022, July). *Solid Gravity Energy Storage: A review* (Vol. 53). Retrieved 6 October 2024, from https://www.researchgate.net/publication/361785221_Solid_Gravity_Energy_Storage_A_review doi: 10.1016/j.est.2022.105226

Tong, W., Lu, Z., Sun, J., Zhao, G., Han, M., & Xu, J. (2022, November). Solid gravity energy storage technology: Classification and comparison. *Energy Reports*, *8*, pp. 926–934. Retrieved 15 September 2024, from https://www.sciencedirect.com/science/article/pii/S2352484722022211 doi: https://doi.org/10.1016/j.egyr.2022.10.286

Urone, P. P., Hinrichs, R., Dirks, K., Sharma, M., Podolak, K., & Smith, H. (2022). *College Physics 2e.* Retrieved 12 July 2024, from https://assets.openstax.org/oscms-prodcms/media/documents/College_Physics_2e-WEB_7Zesafu.pdf

U.S. Department of Energy. (2023, February 28). *How Lithium-ion Batteries Work.* Retrieved 12 December 2024, from https://www.energy.gov/energysaver/articles/how-lithium-ion-batteries-work

U.S. Energy Information Administration. (2024, May 24). *Photovoltaics and electricity.* Retrieved 20 July 2024, from https://www.eia.gov/energyexplained/solar/photovoltaics-and-electricity.php

Wang, W., Yuan, B., Sun, Q., & Wennersten, R. (2022, August 1). *Application of energy storage in integrated energy systems — A solution to fluctuation and uncertainty of renewable energy.* Retrieved 13 May 2024, from https://www.sciencedirect.com/science/article/abs/pii/S2352152X22008210

Wetzel, A. (2019). *Physics Formulary* (3rd ed.). Basel: Adrian Wetzel.

Widmann, E., Schmidt, H., & Rietz, H. (2022, June 22). *E-Auto, Handy und die Energiewende: Sie alle nutzen Lithiumionen-Akkus. Das sind ihre Probleme – und so werden sie besser.*

Retrieved 9 October 2024, from https://www.nzz.ch/wissenschaft/batterien-fuer-elektroautos-herstellung-rohstoffe-problemkreise-ld.1679103

Yue, M., Lambert, H., Pahon, E., Roche, R., Jemei, S., & Hissel, D. (2021). Hydrogen energy systems: A critical review of technologies, applications, trends and challenges. *Renewable and Sustainable Energy Reviews*, *146*, 111180. Retrieved 9 October 2024, from https://hal.science/hal-03221850 doi: 10.1016/j.rser.2021.111180

Zahoransky, R., Allelein, H.-J., Bollin, E., Schelling, U., Schwarz, H., & Wörsdörfer, D. (2019). *Energietechnik* (8th ed.). Wiesbaden: Springer Vieweg.

Zohuri, B. (2016). Electricity, an Essential Necessity in Our Life. In *Application of Compact Heat Exchangers For Combined Cycle Driven Efficiency In Next Generation Nuclear Power Plants: A Novel Approach* (pp. 17–35). Cham: Springer International Publishing. Retrieved 16 May 2024, from https://doi.org/10.1007/978-3-319-23537-0_2 doi: 10.1007/978-3-319-23537-0_2

I hereby declare that the submitted paper is the result of my own, independent work. All external sources are explicitly acknowledged within the paper.